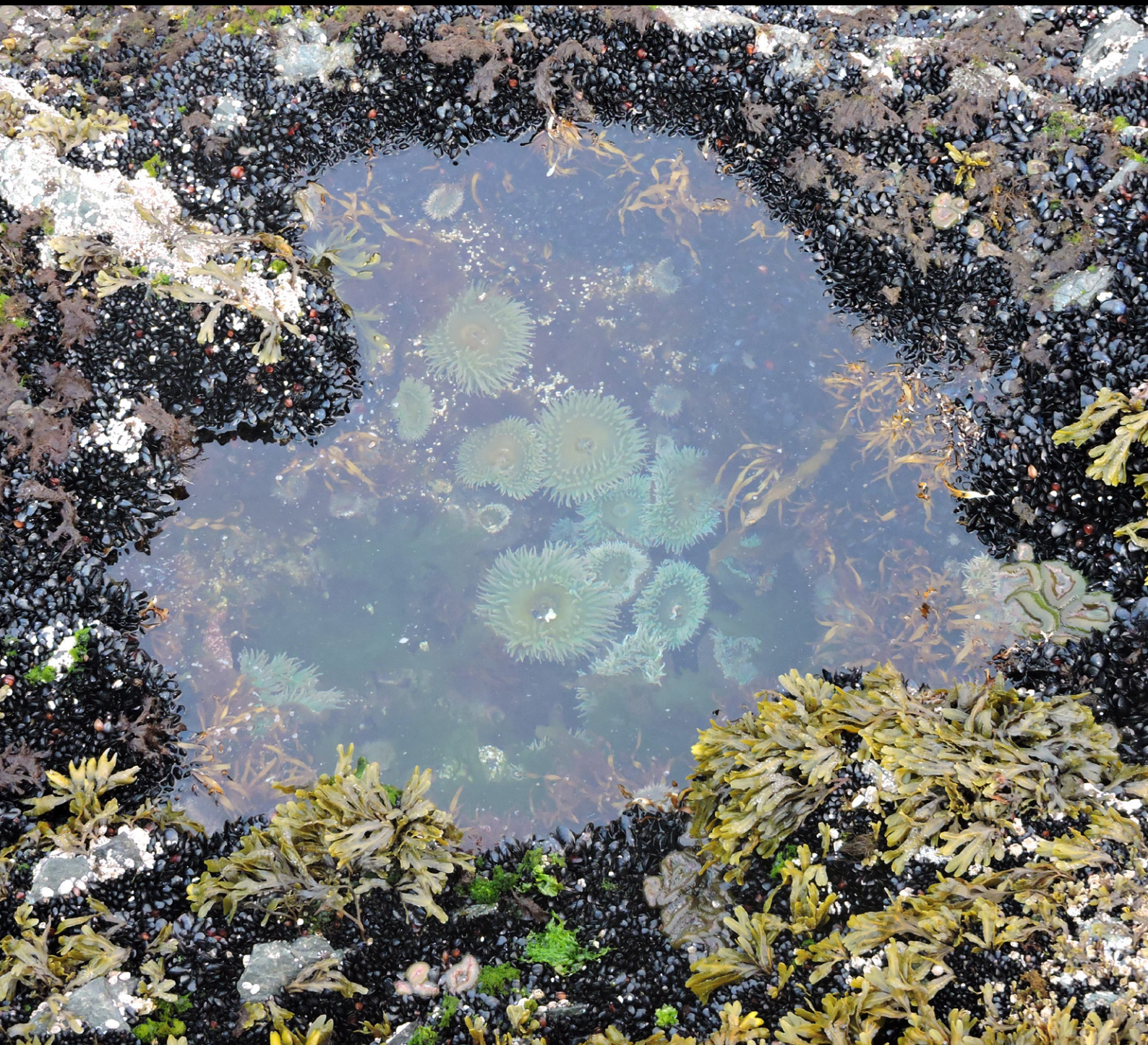


Regional Report
for PICES Region:

11

PICES SPECIAL PUBLICATION 7

Marine Ecosystems of the North Pacific Ocean 2009–2016



PICES North Pacific Ecosystem Status Report, Region 11 (California Current System)

W.J. Sydeman¹

*Farallon Institute, Petaluma, CA USA wsydeman@faralloninstitute.org

Contributing Authors:

S.A. Thompson¹, S. Batten², E. Bjorkstedt³, S. Bograd⁴, R. Brodeur⁵, J. Field⁶, J. Fisher⁷, M. Galbraith⁸, M. Garcia-Reyes¹, R. Goericke⁹, C. Harvey¹⁰, M. Jacox⁴, J. Jahncke¹¹, T. Jones¹², M. Kahru⁹, J. Lanksbury¹³, B. Lavaniegos¹⁴, S. Lippiatt¹⁵, S. Melin¹⁶, Roberta Robertson¹⁷, I. Schroeder⁴, R. Suryan¹⁸, A. Thompson¹⁹, and P. Warzybok¹¹

1 Farallon Institute, Petaluma, CA USA

2 PICES Secretariat, Sydney, B.C. Canada

3 NOAA-NMFS-SWFSC, Trinidad, CA USA

4 NOAA-NMFS-ERD, Monterey, CA USA

5 NOAA-NMFS-NWFSC, Newport, OR USA

6 NOAA-NMFS-SWFSC, Santa Cruz, CA USA

7 Oregon State University, Newport, OR USA

8 DFO-Canada, Sydney, B.C. Canada

9 UC San Diego-Scripps, Institution of Oceanography, La Jolla, CA USA

10 NOAA-NMFS-NWFSC, Seattle, WA USA

11 Point Blue Conservation Science, Petaluma, CA USA

12 University of Washington, Seattle, WA USA

13 Washington Dept Fish Wildlife, Olympia, WA USA

14 CICESE, Ensenada, MX

15 NOAA-Marine Debris, Silver Spring, MD USA

16 NOAA-NMFS-NMML, Seattle, WA USA

17 Humboldt State University, Arcata, CA USA

18 NOAA-NMFS-AFSC, Juneau, AK USA

19 NOAA-NMFS-SWFSC, La Jolla, CA USA

1. Highlights

- weak El Niño event, 2010,
- record coastal upwelling, 2013,
- record ocean warming, 2014–2016
- recent shifts to smaller zooplankton communities
- collapse of anchovy and sardine “forage fish” stocks
- unusual mortality events of seabirds and marine mammals, especially in 2014-2016
- poor annual productivity of seabirds and salmonid populations

2. Introduction

This chapter updates pelagic ecosystem indicators for the California Current System (PICES Region 11, Figure R11-1), focusing on the decade 2009–2018. The main physical oceanographic highlights for this period include, in chronological order, a weak El Niño event in 2009-2010, record upwelling intensity in 2013, and an unprecedented marine heat wave from 2014–2016 which involved both extra-tropical (2014) and tropical, ENSO-related warming (2015–2016). Overall, interannual variability in physical conditions in the region appears to be increasing. The resulting biological impacts have been substantial, including shifts in zooplankton community structure to smaller, less nutritious species due in part to changes in chl-a concentrations, collapse of stocks of forage fish, notably California anchovy and sardine at the same time, and reductions in the size classes of euphausiid crustaceans. Changes in the abundance and/or availability of these mid trophic level species led to major mortality events of the seabirds Cassin’s auklet and common murre during the winters of 2014–2015 and 2015–2016, respectively, and marine mammals/California sea lion pups from 2009–2013), and generally poor productivity of seabirds and salmon across the period. In 2017–2018, the ecosystem began to show signs of recovery with stronger upwelling, cooler temperatures and strong productivity of anchovy, some other forage fish, and euphausiids.

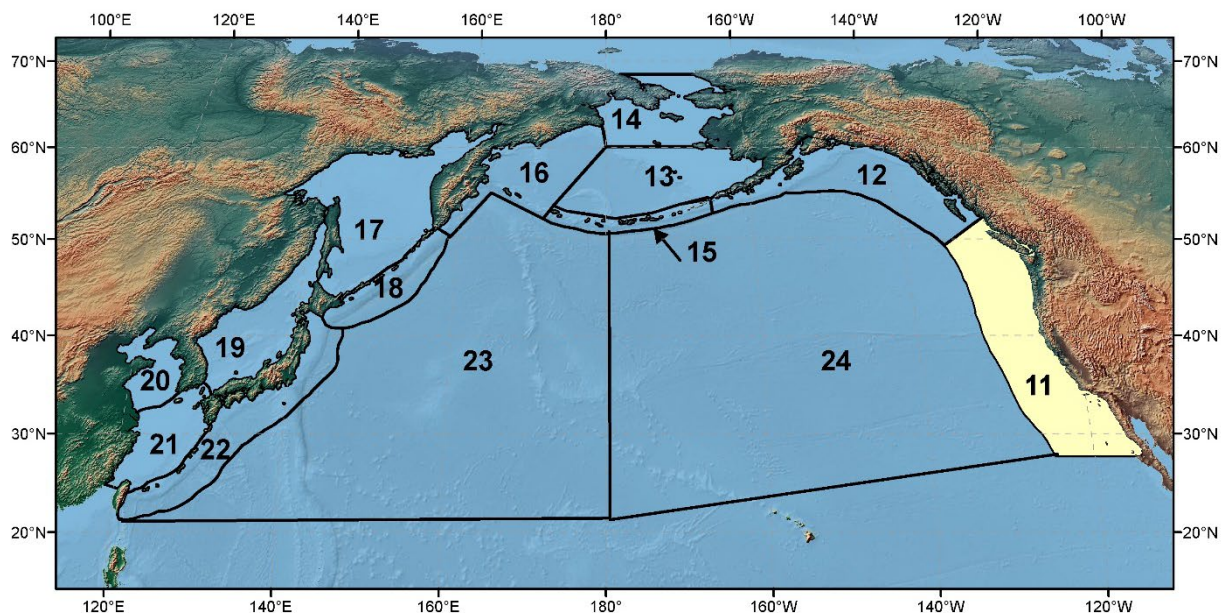


Figure R11-1. The PICES biogeographical regions and naming convention for the North Pacific Ocean with the area discussed in this report highlighted.

3. Physical Ocean

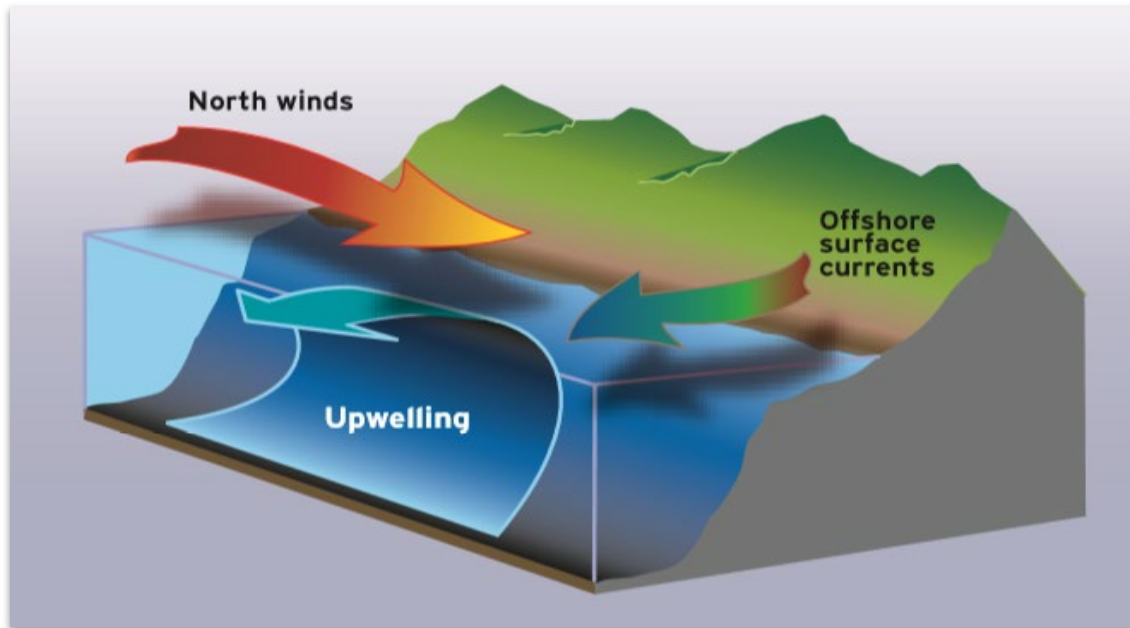


Figure R11-2. Schematic of wind and current function in the California Current Upwelling Ecosystem.

3.1 Basic Ecosystem Functions

Region 11 productivity is strongly controlled by “bottom-up” processes that begin with upwelling, the vertical transport of nutrient-rich cold waters into the sunlit euphotic zone of the coastal ocean (Figure R11-2). Upwelling is driven by northwesterly winds coupled with the Coriolis force, resulting in offshore and vertical advection (Huyer 1983). Upwelling in the region is highly variable in space because of bathymetry and topography that cause spatially-segregated “upwelling jets” to form offshore of coastal promontories and along the shelf break (Chhak and Di Lorenzo 2007). In relation to nutrient input, the efficacy of upwelling varies in time and is related to ocean warming, which increases stratification and impedes vertical mixing. Stratification partly explains reduced primary productivity in the ecosystem during ENSO years. Upwelling may increase with global warming (Bakun 1990), but the mechanism of change is uncertain (Ryckaczewski et al. 2015) and observations to date are equivocal due to difficulties in separating unidirectional trends from interdecadal variability (Sydeman et al. 2014).

3.2 Spatial Variability in Productivity

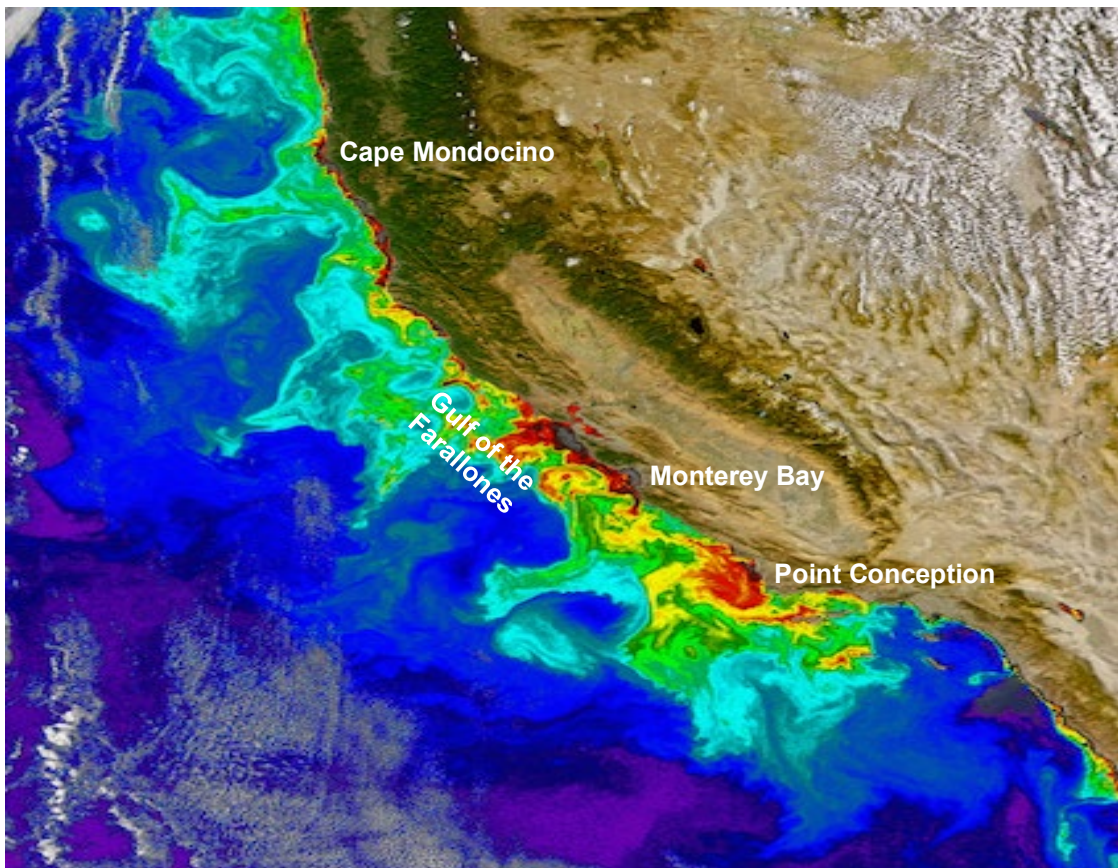
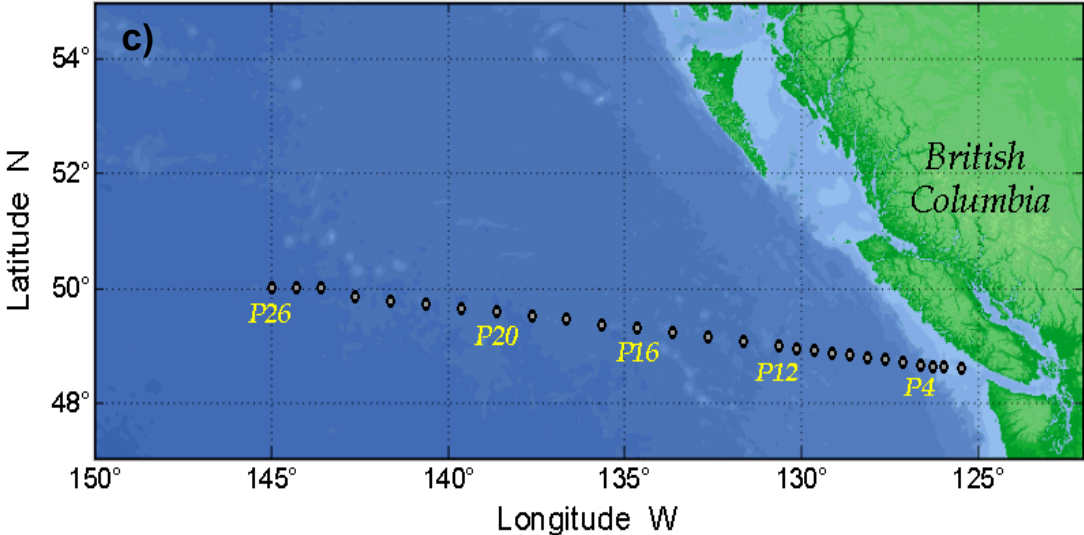
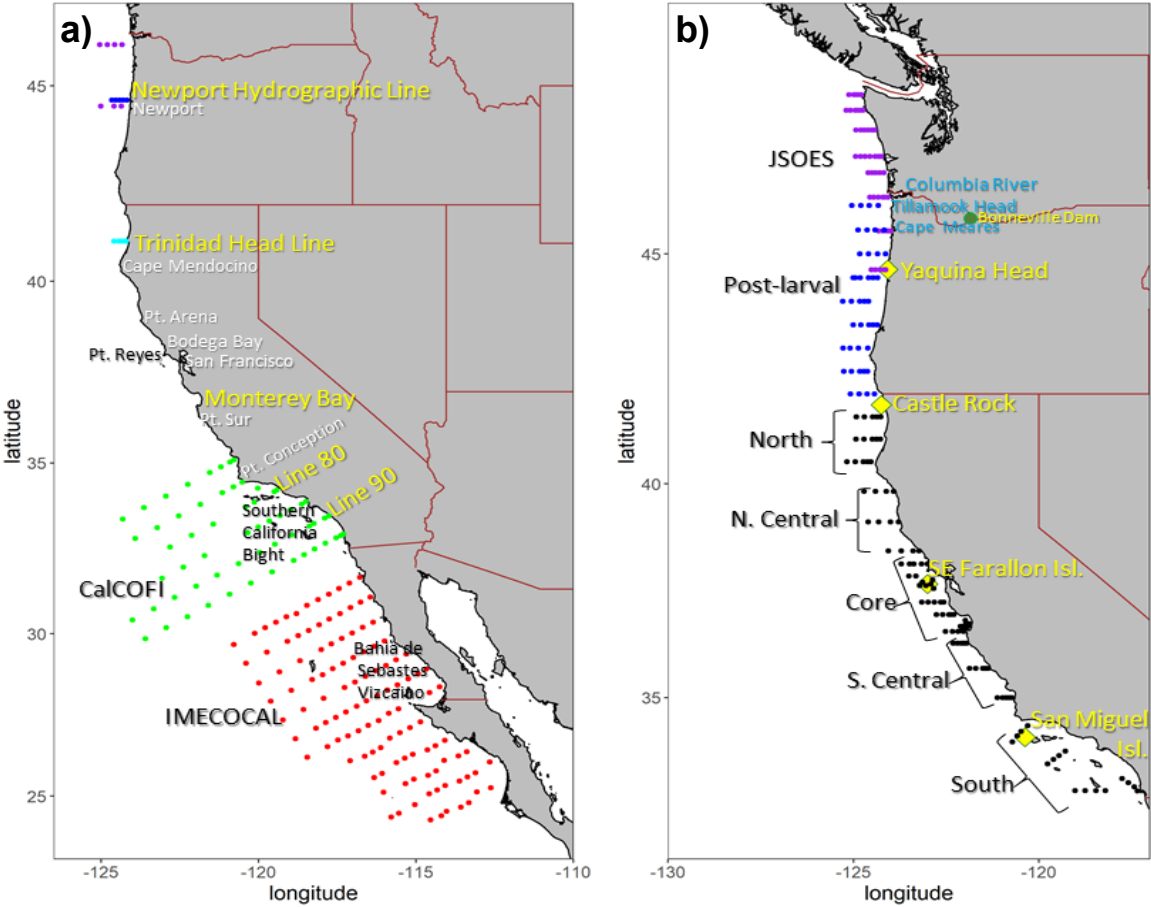


Figure R11-3. Satellite image of mesoscale variability in surface chl-a concentration in R11. Warm colors indicate higher chl-a concentrations.

Spatial variability in coastal topography and upwelling results in substantial mesoscale variability in primary productivity, as is evident from a 21 September, 2004, SeaWiFS-based satellite image of chl-a concentrations (Figure R11-3). In this image, productivity is greatest along the central California coastline and there are mesoscale “hotspots” of chl-a concentrations very near the coastline, immediately north of Point Conception, in Monterey Bay, and in the wide shelf region of the Gulf of the Farallones with extensions to ~100 km offshore. The structuring of the chl-a field also is related to coastal upwelling jets at Cape Blanco, Oregon, and Cape Mendocino, Point Arena, Point Sur, and Point Conception, California. The ecosystem may therefore be considered by its three primary eco-regions: the Southern California Bight south of Point Conception, the central California Current region from Point Conception to Cape Mendocino, and the northern California Current region north of Cape Mendocino (GLOBEC 1992). Effectively, changes in the ecosystem can thus be described by observations off (1) Southern California, (2) Central-Northern California, and (3) Oregon to Southern British Columbia including the west coast of Vancouver Island, where upwelling may also be substantial (Foreman et al. 2011).

3.3 Sampling Programs



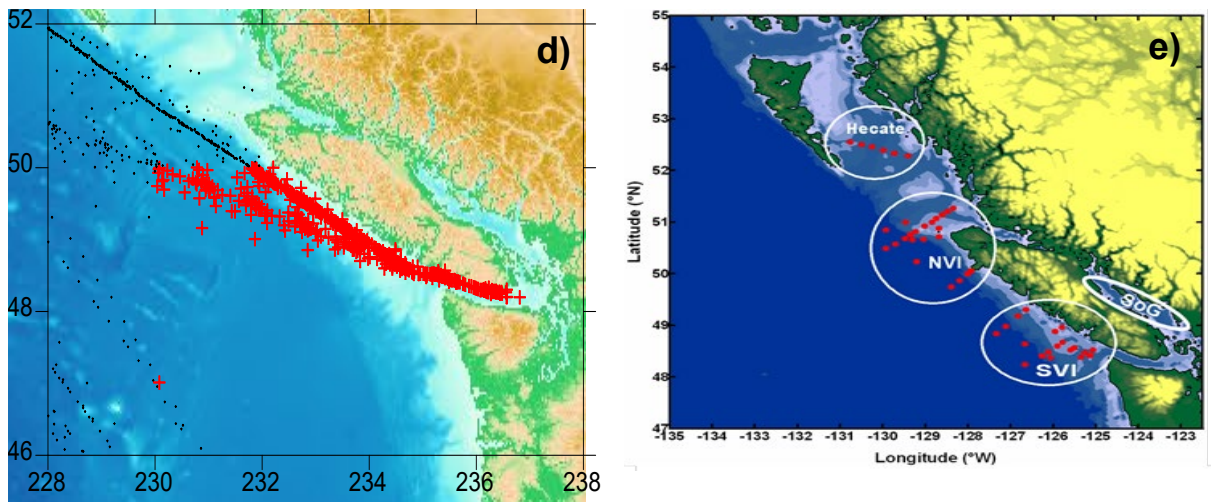


Figure R11-4. Sampling programs in Region 11. a) California Cooperative Oceanic Fisheries Investigations (CalCOFI) and related IMECOCAL programs, b) Juvenile and post-larval fish survey, and seabird and marine mammal monitoring, c) Line P program, d) Pacific Continuous Plankton Recorder project and e) Department of Fisheries and Oceans Canada (DFO) Zooplankton Studies Program (NVI and SVI: northern and southern Vancouver Island, SoG: Strait of Georgia)

Physical and biological sampling programs in Region 11 are substantial in spatial and temporal coverage (Figure R11-4), though information gaps remain, particularly for wintertime observations. The backbones of the ocean observation system (OOS) in the California Current Ecosystem include the California Cooperative Oceanic Fisheries Investigations (CalCOFI) and related IMECOCAL programs off Southern California and Baja California (Figure R11-4a) and the Line P program off British Columbia (Figure R11-4c). All of these programs were initiated in the early 1950s and have continued, more or less at seasonal to annual time scales, since that time (Pena and Bograd 2007). These programs were initiated to study and understand population fluctuations, particularly the collapse of fisheries stocks (notably sardine, *Sardinops sagax*), and include physical, biological (fish eggs and larvae), and chemical oceanographic observations. These large-scale programs have been recently supplemented with coastal transects including the Newport Hydrographic Line (Oregon) and the Trinidad Head Line (northern California), with observations begun in the mid 1990s (Figure R11-4a). Studies of juvenile fish recruitment are conducted along the coastline as part of the Rockfish Recruitment and Ecosystem Assessment Survey (RREAS; Sakuma et al. 2016; denoted as South, South-Central, Core, North-Central, and North in Figure R11-4b), Post-Larval Survey, and the Juvenile Salmon Ocean Ecology Survey (JSOES) off Oregon and Washington (Figure R11-4b). In addition to the Line P program, the Pacific Continuous Plankton Recorder project collects data along the west coast of Vancouver Island on a transect that arcs across the North Pacific to Japan (Figure R11-4d), and Department of Fisheries and Oceans Canada (DFO) conducts a Zooplankton Studies Program along the west coast of Vancouver Island and in Hecate Strait (Figure R11-4e). Seabird and marine mammal breeding biology is monitored at Yaquina Head, OR, and Castle Rock, SE Farallon Island, and San Miguel Island, CA (Figure R11-4b).

3.4 Ocean Climate Indices

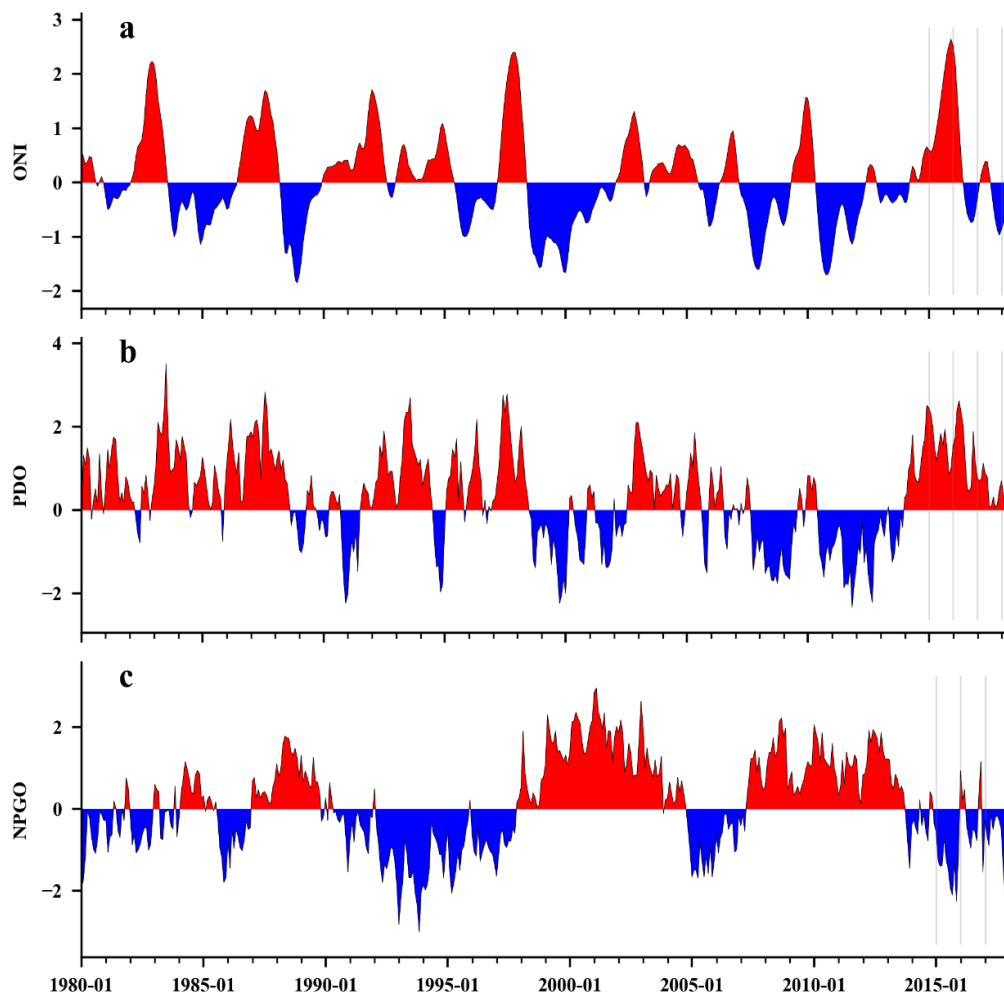
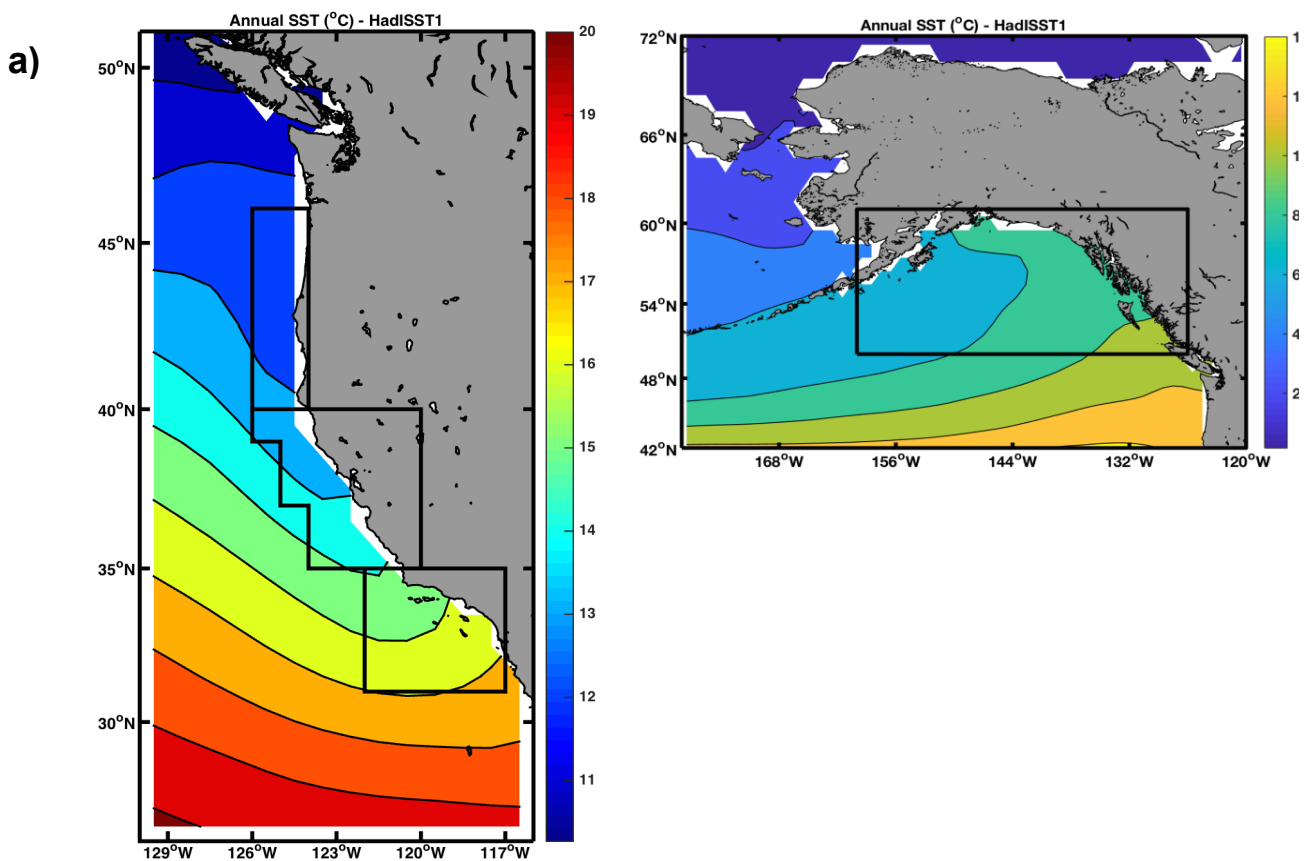


Figure R11-5. Time series of monthly values (January 1980–December 2018) for three ocean climate indices especially relevant to the California Current: a) Oceanic Niño Index (ONI), b) Pacific Decadal Oscillation (PDO), and c) North Pacific Gyre Oscillation (NPGO). Data were obtained from <http://oceanview.pfeg.noaa.gov/erddap/>.

The Oceanic Niño Index (ONI), a three-month running mean of SST anomalies averaged over 5°S–5°N and 120°W–170°W (NINO3.4 region), transitioned from peak El Niño conditions at the start of 2016 to weak La Niña conditions by the end of 2016 (Figure R11-5a). While the 2015–16 El Niño reached ONI values that rivaled those of the record 1997–98 El Niño event, its impact along the US west coast was less pronounced (Jacox et al. 2016). The 2017 ONI values briefly switched to positive during the spring and summer, but they were lower than the 0.5 °C threshold that signifies an El Niño event. Negative ONI values lower than -0.5 °C (the threshold for a La Niña event) occurred starting in October 2017 and lasted until March 2018. Fall 2018 ONI values indicated that temperature anomalies in the NINO3.4 region were conducive for an El Niño to develop. The Pacific Decadal Oscillation (PDO) index describes the temporal evolution of dominant spatial patterns of SST anomalies over the North Pacific (Mantua et al. 1997). Positive PDO values are associated with a shallower upwelling cell in the northern California Current System (CCS) (Di Lorenzo et al. 2008). The PDO was positive for all of 2016 with peak values in the spring and lowest

values in the summer (Figure R11-5b). The April 2016 value of 2.62 was the largest value during the large marine heat wave and El Niño event of 2014–16. Positive PDO values persisted for all of 2017 although these values were low, particularly during the summer. Since February 2018 and through the rest of that year, PDO values have been neutral with values near zero. The North Pacific Gyre Oscillation (NPGO) is a low-frequency signal of sea surface height variations across the North Pacific, indicating variations in the circulation of the North Pacific Subtropical Gyre and Alaskan Gyre (Di Lorenzo et al. 2008). Positive NPGO values are linked with increased equatorward flow in the California Current, along with increased surface salinities, nutrients, and chlorophyll values in the southern-central CCS (Di Lorenzo et al. 2009). Negative NPGO values are associated with decreases in these variables, inferring less subarctic source waters, fewer nutrients, reduced upwelling, and generally lower production in the CCS. The NPGO during 2016 had short-duration positive values in the winter and fall, which were the largest positive values since 2013 (Figure R11-5c). The 2017 NPGO values remained negative throughout the year, with the largest negative values in the fall. In fact, the negative values from October 2017 to December 2018 were a period of some of the largest negative NPGO values for the whole record since 1950.

3.5 Regional Variation in SST, HAD1SST, 1870-2016



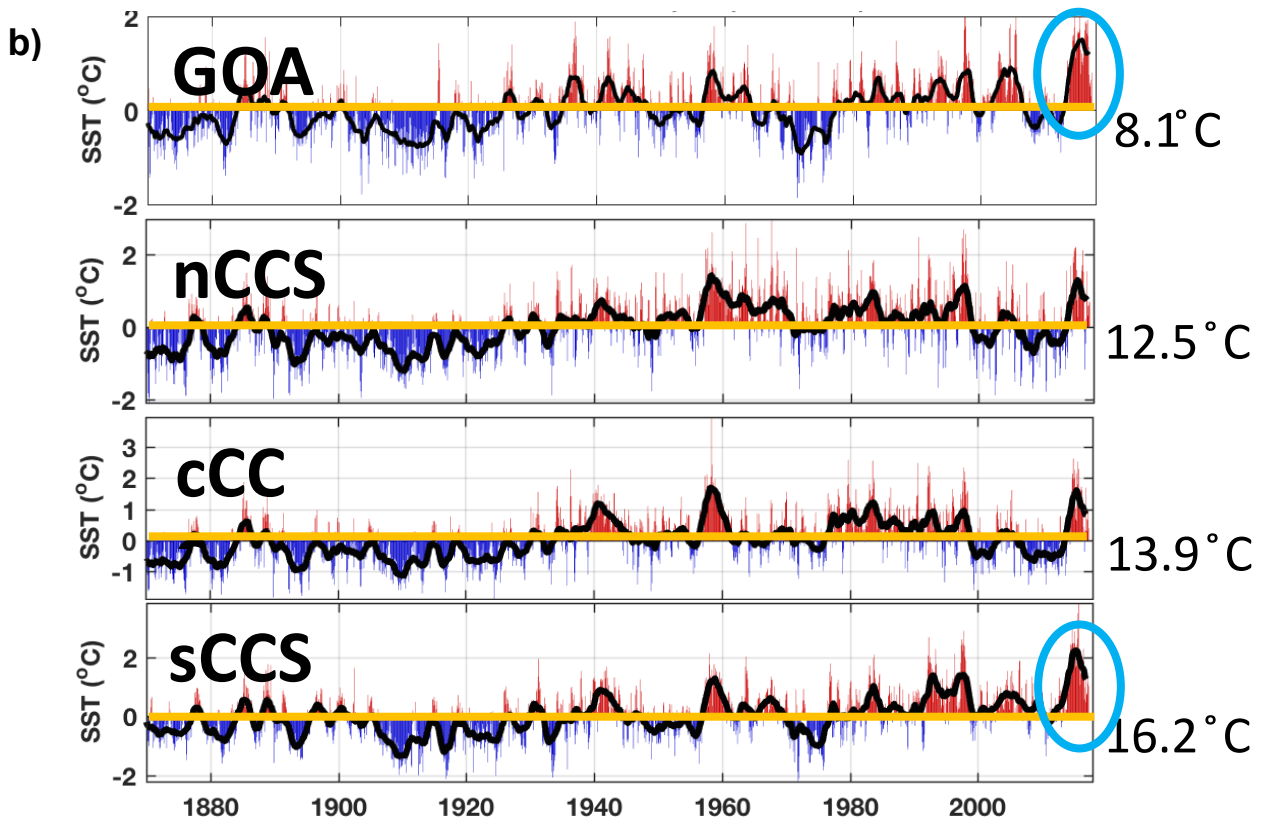


Figure R11-6. Spatial and temporal variation in SST based on the HAD1SST dataset from the late 1800s to 2018, comparing regions for R11 and R12. a) Annual average SST in R11 (left) and R12 (right) and regions for average SST calculation, b) centennial variation of SST anomaly of R11 (nCCS, cCCS, sCCS: northern, central and southern California Current System, respectively) and R12 (GOA: Gulf of Alaska).

The figure R11-6 shows the regions used to assess centennial variation in SST based on the UK Meteorological Office Hadley Centre Hadley1 SST dataset (Burrows et al. 2011). The sub-regions shown are as previously discussed, based on GLOBEC 1992, and delineate the southern, central, and northern California Current System. For comparison, a region of the Gulf of Alaska was also selected. Anomalies in SST in the southern, central, northern CCS, and GoA are illustrated in Figure R11-6b (Garcia-Reyes and Sydeman, unpubl). While data from the late 1800s through ~1920 must be considered with care, a general trend of ocean warming in these regional boxes is evident, as well as pulses of warming in the early 1940s, and during the 1957–1958, 1982–1983, and 1997–1998 ENSO events. The 1980s and 1990s were generally warm. The most extensive warming anomaly on record occurred from 2014–2016 in the southern CCS and GoA. The 2014–2016 warming event, which includes extra-tropical warming known as the “The Blob” (Bond et al. 2015) and a 2015–2016 ENSO was unprecedented in amplitude in these regions (Di Lorenzo and Mantua 2016) but was not unprecedented in either the central CCS or northern CCS. In these regions, warming during the 1957–1958 event was as extensive. In the central and northern CCS, there was a long-term cool period from about 2000–2013, preceding the 2014–2016 marine heat wave. Upwelling was strong throughout the period except during 2005–2006.

2.6 Wind Stress and SST Anomalies from Buoys, California, 1980–2018

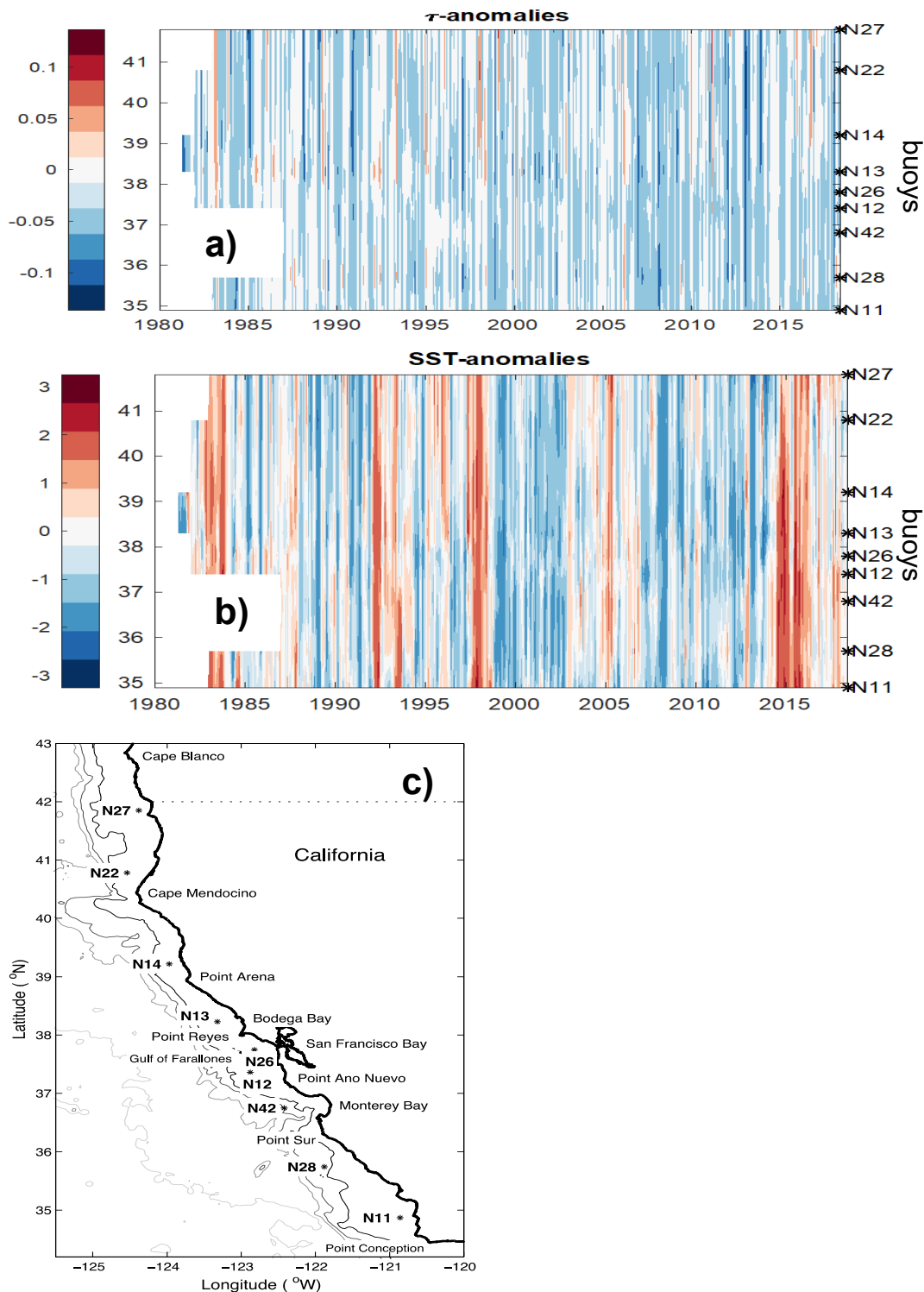


Figure R11-7. Monthly wind a) and temperature b) anomalies based on 9 buoys in central and northern California, 1982–2018. c) Location of the buoys (indicated as N).

Alongshore wind stress (Figure R11-7a, units N/m^2) and sea surface temperature (Figure R11-7b, $^{\circ}\text{C}$) monthly anomalies from NOAA buoys along the central and northern California coast are available since early 1980s to the present (Garcia-Reyes and Largier 2010). Data gaps were filled with data from neighboring buoys. Buoy locations are shown in Figure R11-7c and on the right axes in Figure R11-7a, b. Negative anomalies in wind stress indicate

more upwelling-favorable conditions. Wind stress shows less variability than SST, however, it also shows a period of stronger upwelling-favorable winds along the entire coast in the late 2000s and few years with strong upwelling events in the early 2010s, especially in 2013. A decrease in positive alongshore anomalies (weaker upwelling) south of N13 (Bodega Bay) is observed over time. SST anomalies show the widespread effect of El Niño events in 1983, 1992, 1997–1998, and the prolonged effect of the marine heat wave in 2014–2016 related to The Blob and the 2015–2016 ENSO event.

3.7 Wind Stress and SST Anomalies, Monterey Bay, 1987–2018

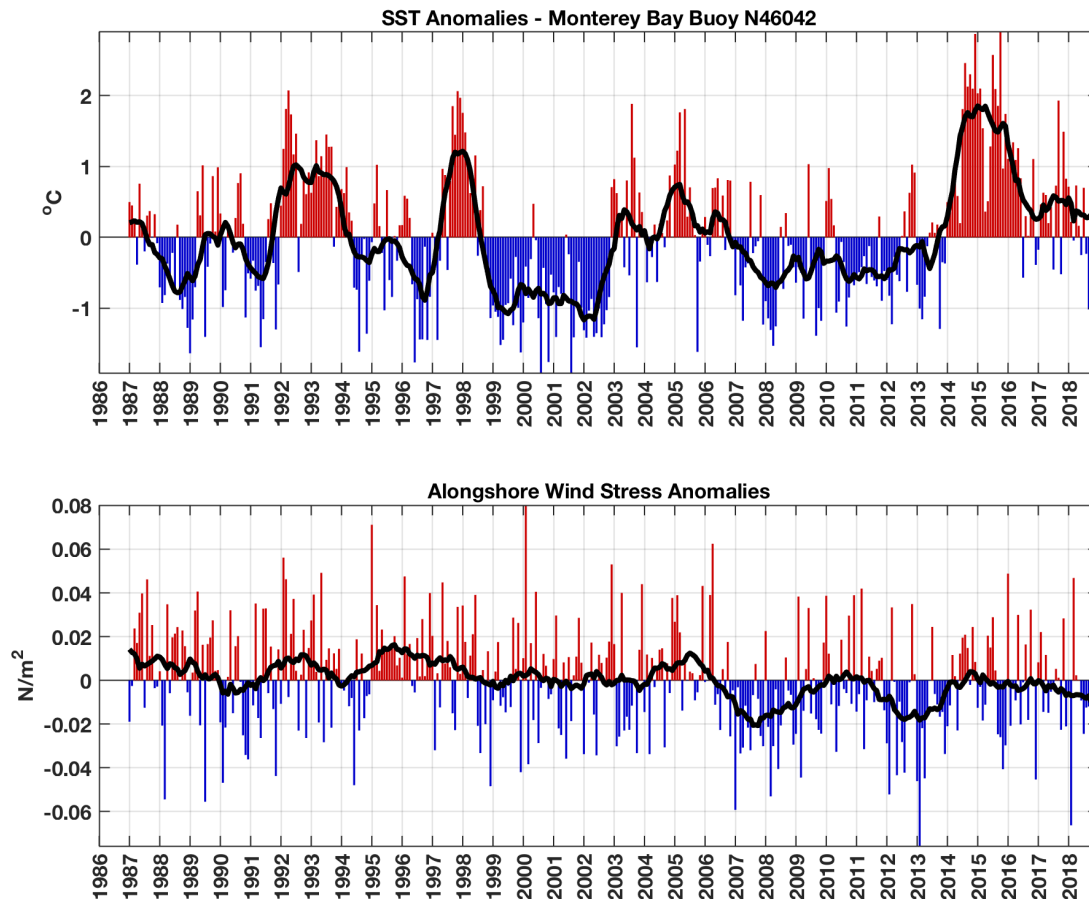


Figure R11-8. Monthly temperature (top) and wind (bottom) anomalies based on a buoy in Monterey Bay, in central California, 1987–2018.

SST and alongshore wind stress anomalies for NOAA buoy 46042 at Monterey Bay in central California are shown in Figure R11-8. Interannual variability in SST is the most pronounced characteristic at this buoy, though this variability was not always associated with variability in upwelling-favorable winds (Garcia-Reyes and Largier 2010). Stronger upwelling winds were measured in the period 2007–2010 and again 2012–2014; while SST anomalies were also negative, they were not as pronounced as those between 1999–2002. The extreme and prolonged positive anomalies in SST in 2014–2016 do not correspond to non-normal anomalies for wind. Despite normal upwelling-favorable winds, SST anomalies continue after 2016, although they were smaller than in 2014–2016. Though still warm, SST anomalies from this site indicate a return to more normal conditions in 2017–2018. Upwelling winds also increased in the last two years.

3.8 SST and Upwelling Indices by latitude, 2014–2018 (Figure R11-9)

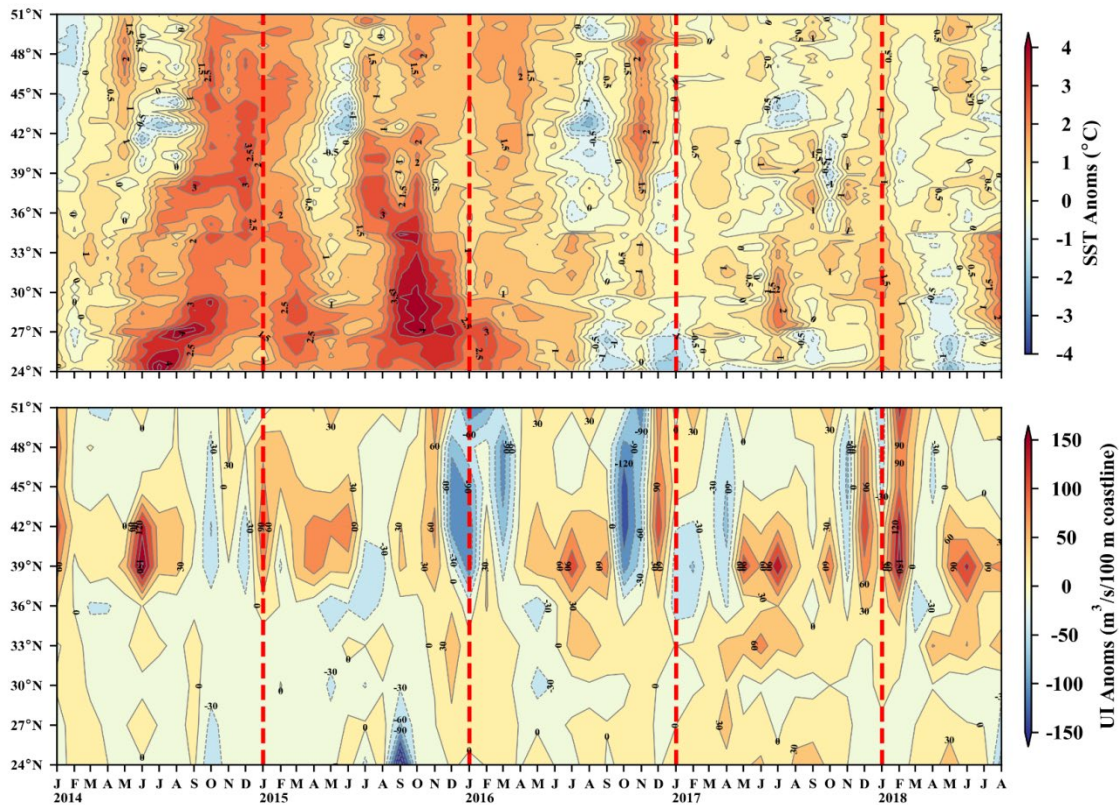


Figure R11-9. Monthly sea surface temperature (SST) anomalies (top) and upwelling index (UI) anomalies (bottom) for January 2014–December 2018 between 24–48°N relative to 1982–2018 monthly means. The SST anomalies were averaged from the coast to 100 km offshore. Positive and negative upwelling anomalies denote greater than average upwelling or downwelling (usually during the winter), respectively. Daily optimum interpolation AVHRR SST data were obtained from <http://coastwatch.pfeg.noaa.gov/erddap/griddap/ncdcOisst2Agg>. Six-hourly upwelling index data were obtained from <http://oceanview.pfeg.noaa.gov/erddap/>.

High SST anomalies due to the marine heat wave and El Niño event were evident from spring 2014 to summer 2016. Positive SST anomalies (>1 °C) persisted during the winter and spring of 2016, especially for locations north of 42°N and south of 30°N. From January–May 2017, SST anomalies north of 42°N were near the long-term average, with the exception of a few localized periods of ~ 0.5 °C anomalies. Positive SST anomalies were higher for latitudes south of 42°N and a few locations experienced anomalies greater than 1°C during summer/fall 2017. January 2018 SST anomalies were 0.5 to 1 °C warmer than average for all latitudes. A slight drop in temperature anomalies, to near climatological values, occurred in February–March 2018. Temperature anomalies were less than 1 °C for latitudes north of 36°N from June–December 2018. In the winter 2015–2016, upwelling anomalies were negative north of 33°N (Figure R11-8), which is typical of past El Niño winters, but were positive at 33°N and south, which is atypical and contributed to a relatively muted impact of the 2015–16 El Niño off California (Frischknecht et al. 2017). The most upwelling-favorable anomalies during 2016 occurred from July–September for latitudes 36–42°N, followed by strong downwelling anomalies in October and November 2016 north of 36°N. The largest negative upwelling anomalies in early 2017 were for latitudes 36–45°N.

Upwelling during May–October 2017 was generally average to above average for the whole coast with the largest positive anomalies in late spring/early summer. Upwelling anomalies were generally positive for the majority of 2018. Large positive upwelling anomalies occurred for latitudes 39–42°N at the beginning of 2018.

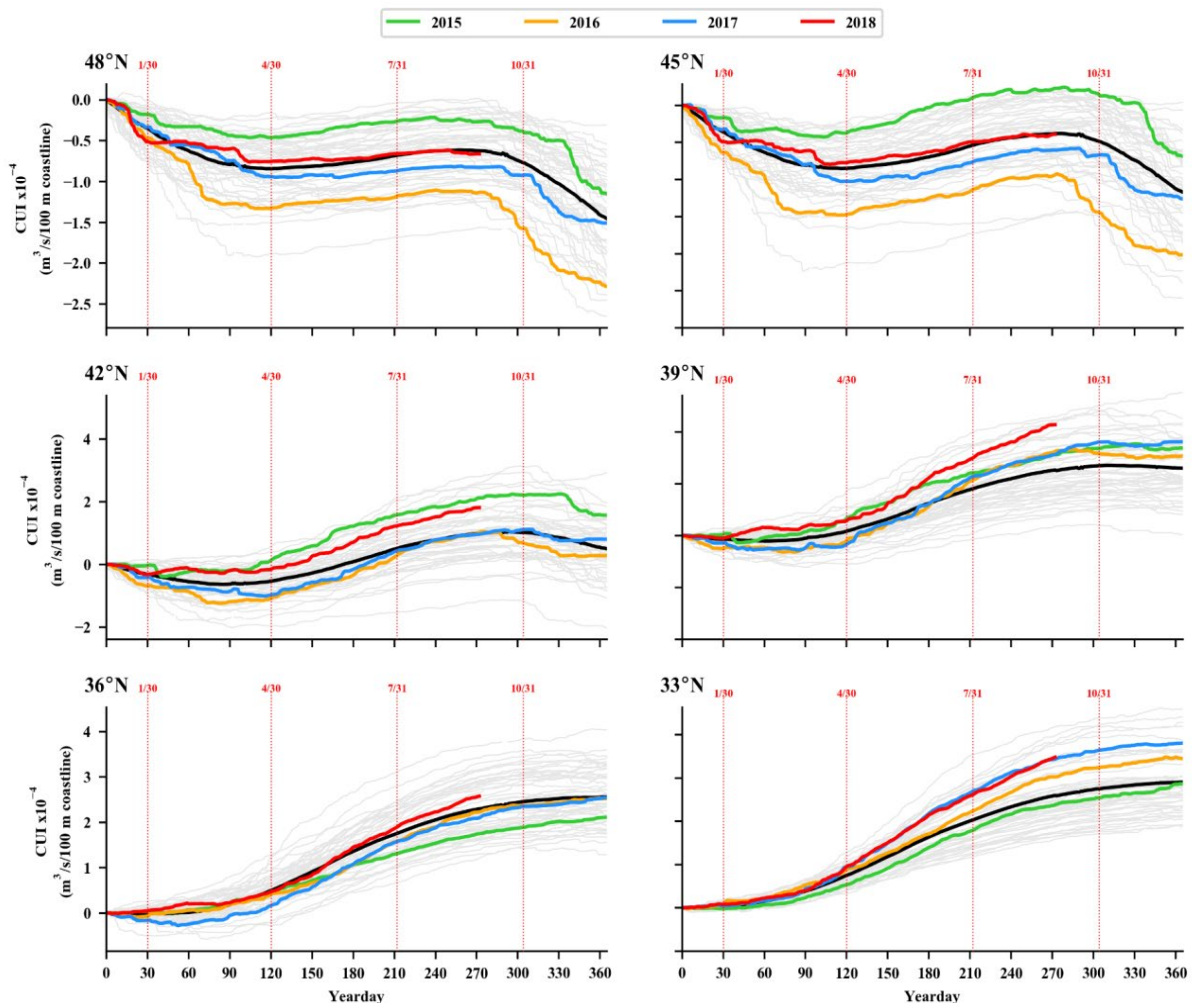


Figure R11-10. Cumulative Upwelling Index (CUI) starting on January 1 calculated from the daily upwelling index at locations along the west coast of North America. Grey lines are annual CUI for 1967–2014 and colored CUI curves are for 2015–2018. The black line is the CUI climatological mean. The red dashed vertical lines mark the end of January, April, July, and October. Daily upwelling index data were obtained from <http://oceanview.pfeg.noaa.gov/erddap/>.

3.9 Daily Cumulative Upwelling Index by latitude, 2015–2018

The cumulative upwelling index (CUI) is the cumulative sum of the daily UI values starting January 1 and ending on December 31, and it provides an estimate of the net influence of upwelling on ecosystem structure and productivity over the course of the year (Bograd et al. 2009). In general, upwelling in winter and spring was slightly stronger in 2018 than the previous two years (Figure R11-10). During winter 2016, upwelling north of 39°N was low due to the El Niño and strong upwelling only began in the summer. South of 39°N, upwelling anomalies were neutral to positive in early 2016, counter to what would be expected from a strong El Niño (Jacox et al. 2015). Upwelling in 2017 was near the long-term average for the whole coast except for the latitudes 36–42°N. For these latitudes, the CUI curves in winter were below the climatological curve and upwelling began in early May. Strong upwelling in February 2018 pushed the CUI curves above the long-term average, however, downwelling

started in April and dropped the CUI curves towards the long-term average for latitudes 36°N and 45–48°N. Upwelling was especially strong for latitudes 39–42°N in 2018.

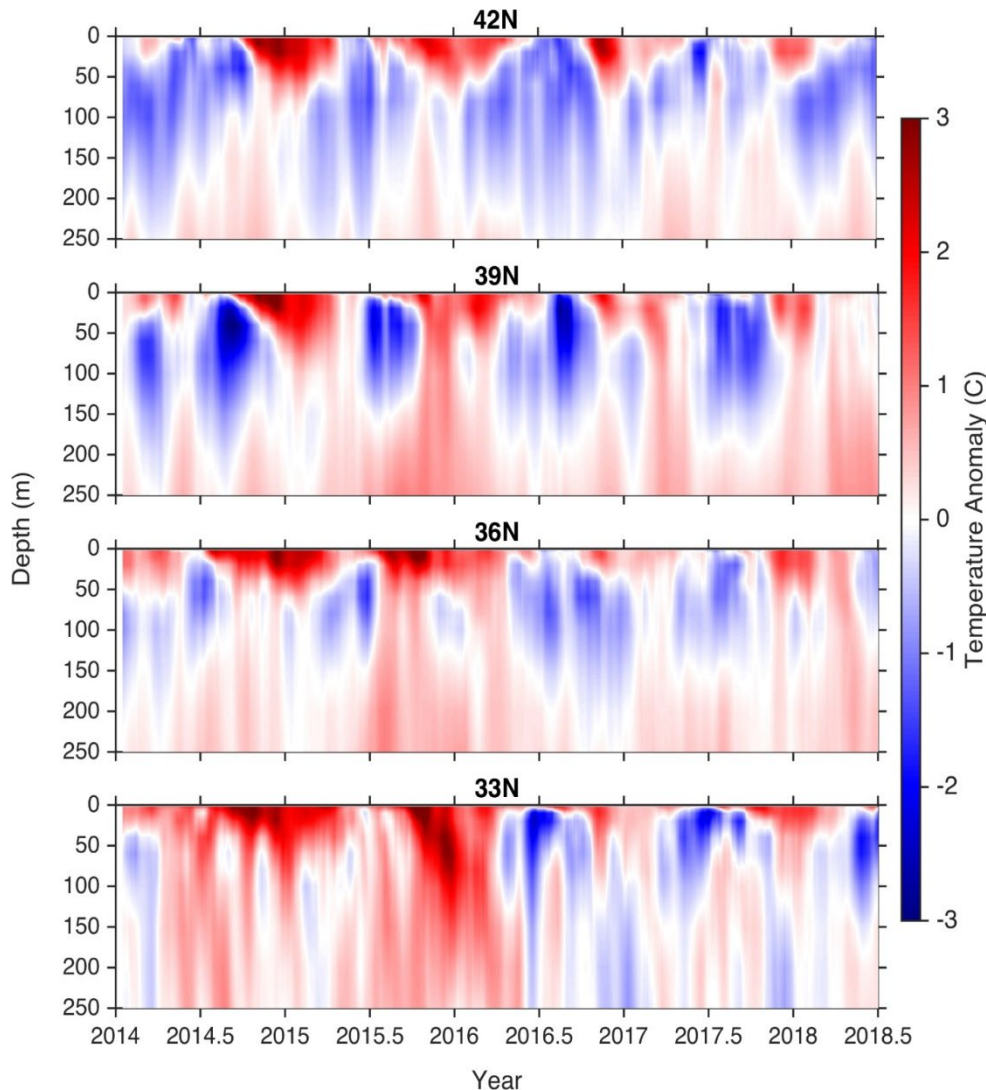


Figure R11-11. Water column (0–250 m) temperature anomalies (°C) relative to the 1999–2011 climatology along 33°N, 36°N, 39°N and 42°N), derived from a data assimilative ocean reanalysis of the California Current System (Neveu et al. 2016; <http://oceanmodeling.ucsc.edu/ccsnrt/>), are shown at four latitudes off the US West Coast. Temperatures were averaged from the coast to 100 km offshore and smoothed with a 30-day running mean.

3.10 Temperature Anomalies by Depth, Data Assimilative ROMS, 2014–2018

The signature of the northeast Pacific marine heat wave was evident in temperature anomalies by depth (0–250 m) at all latitudes beginning in 2014, and was particularly prominent in the winters of 2014–2015 and 2015–2016. Nearshore (within 100 km of the coast) temperature anomalies were surface intensified, with the most intense warming concentrated in the upper 50 m (Figure R11-11). At more southern latitudes particularly in the Southern California Bight, (along 36 and 33°N in Figure R11-11), warm anomalies penetrated deeper in the water column, an effect that was most pronounced in the winter of 2015–2016 when the lingering impact of the preexisting warm anomaly (Zaba and Rudnick 2016) was augmented by a strong El Niño and associated ocean forcing through the coastal waveguide (Jacox et al. 2016, Frischknecht et al. 2017, Rudnick et al. 2017). A brief cooling of nearshore temperatures in spring 2015 was evident at all latitudes and was driven by an

anomalously strong upwelling season in the midst of the broader warm anomaly (e.g., Peterson et al. 2017). Since mid-2016, temperatures generally cooled throughout much of the CCS, though elevated surface temperatures recurred in winter perhaps due to the “reemergence mechanism”, in which warm anomalies persist at depth through spring/summer and reemerge when the mixed layer deepens in winter (Alexander et al. 1999).

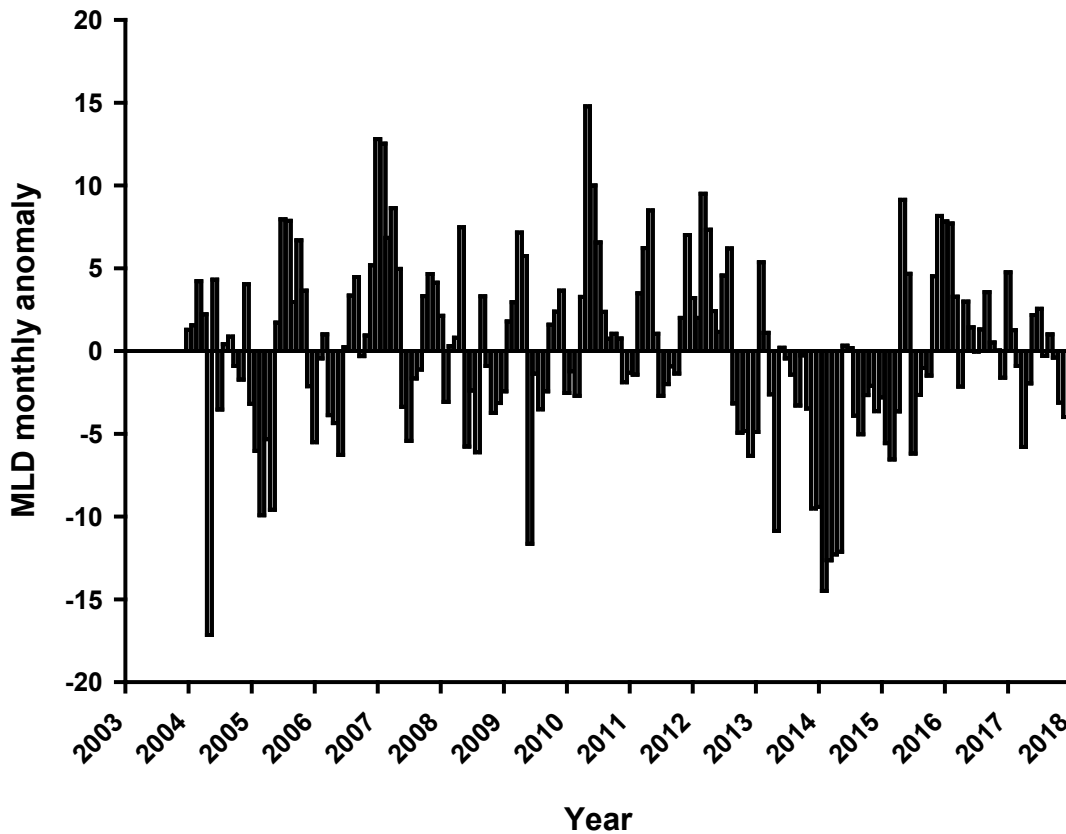


Figure R11-12. Monthly mixed layer depth anomalies (m) measured by Argo sensors in R11, 2004–2018.

3.11 Monthly Mixed Layer Depth Anomalies, Argo Sensors, 2004–2018

Mixed layer depth (MLD) as measured by Argo sensors from 2004–2018 are presented here as monthly anomalies (Figure R11-12). Considerable variability in mixed layer depth was evident with deeper MLD in 2007–2008 and 2011–2013. The most notable feature in this time series is the signature of the marine heat wave from 2014–2016, which resulted in shallow MLD for many sequential months. Lack of vertical mixing was a strong characteristic of that event, and the resulting mixed later depth showed negative anomalies. MLD reversed somewhat in 2017 and remained close to the mean value.

4. Chemical Ocean

4.1 Oxygen Concentration, Southern British Columbia, 1980–2013

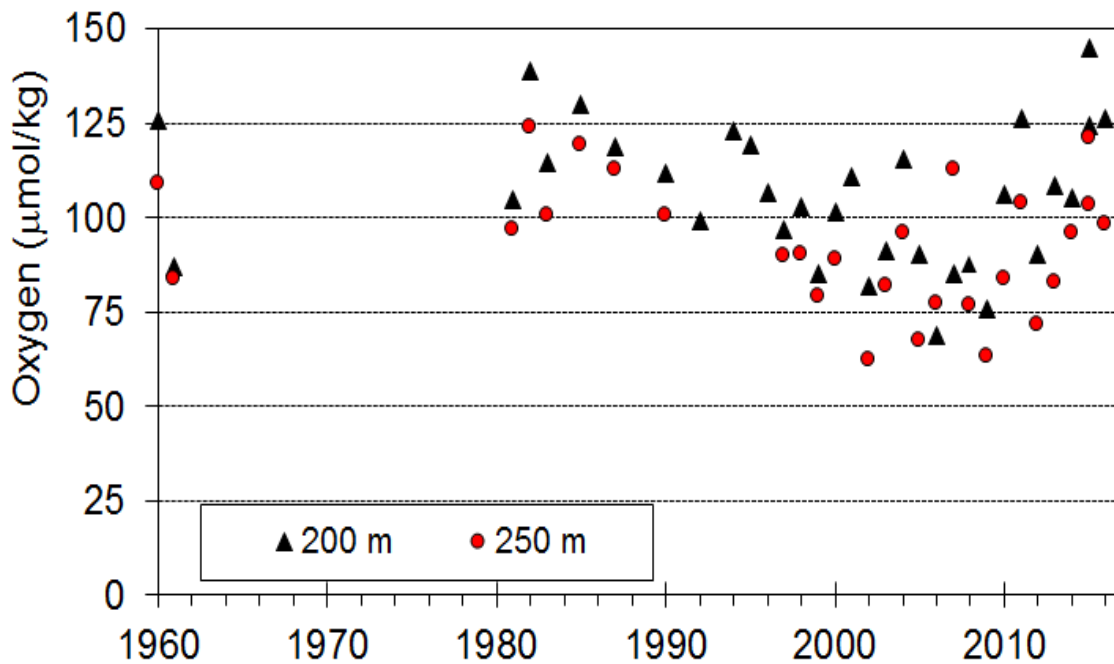


Figure R11-13. Summer (August or September) oxygen concentration at Station P4 of Line P, Southern British Columbia, 1980–2013.

Oxygen concentration (O_2 , $\mu\text{mol/kg}$) at depths of 200 and 250 m at Station P4 of Line P (Figure R11-4c), a continental slope station, is shown in Figure R11-13. Only measurements from August or September (summer) are included (updated from Crawford and Peña 2013). The data reveal minimum O_2 in the summers of 2002 and 2009, together with a general decreasing trend from 1980s to 2000s, and an increasing trend after 2009. The few observations in the early 1960s suggest lower O_2 than observed in the 1980s, however, there are too few observations at 200 and 250 m at P4 to determine if the increase from 1960s to 2000s is significant. The changes in O_2 on the continental slope at P4 are likely due to changes in winds along the west coast of Vancouver Island in 2012–2013. The increase in O_2 after 2009 at Station P4 is welcome news.

4.2 Mixed Layer chl-a, Nitrates, and Nutricline Anomalies, Southern California, 1985–2018

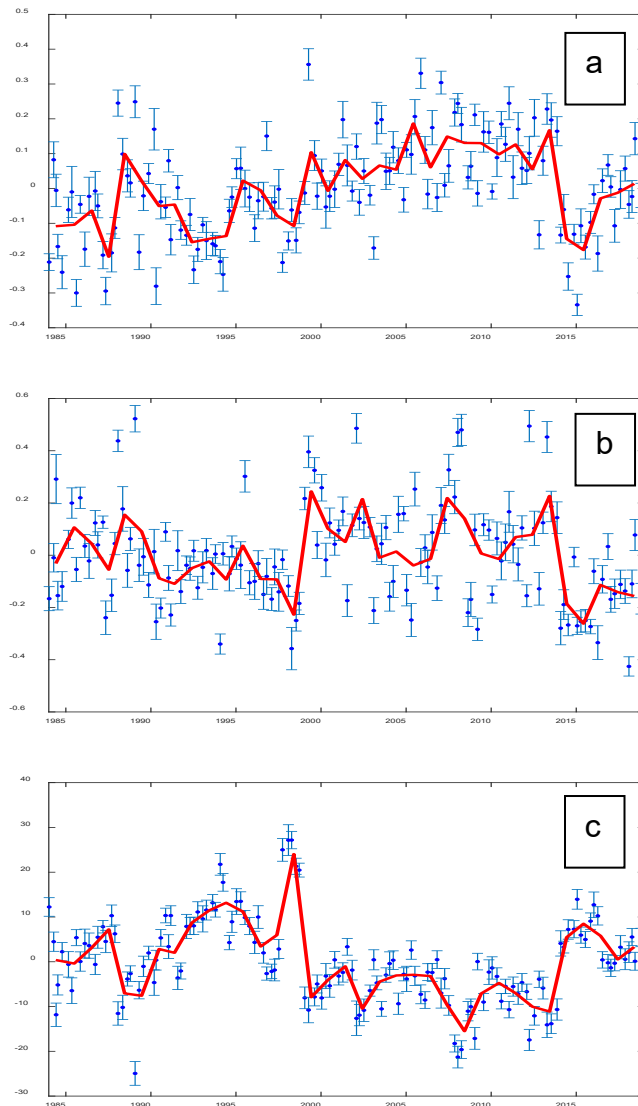


Figure R11-14. Anomalies in mixed layer (a) chl-a concentrations, (b) nitrate, and (c) depth of the nitracline Whiskers indicate the 95% confidence intervals for the seasonal means. Red solid lines represent annual averages. Anomalies are based on the seasonal averages from 1984–2012 time period.

Mixed layer (ML) properties within the CalCOFI study area show distinct and mostly synchronous variations with time (Figure R11-14a). Three distinct periods are discernible in the data and are confirmed by change-point analysis: 1984 (the start of the time series) to 1998, 1999 to 2014, and the last four years to 2018 when the system underwent a series of dramatic changes. ML chl-a was low during the first time periods, increased from 1999 until 2013, was extremely low during the recent marine heat wave, and has been close to the long-term average since 2016. Variations of ML nitrate (Figure R11-14b) were similar, except that it remained low during the last three years. The depth of the nitracline (the depth where concentrations of nitrate reach values of $1 \mu\text{M}$; Figure R11-14c), covaried inversely with ML nitrate. These data indicate that phytoplankton biomass in the CalCOFI domain continues to be controlled by the supply of inorganic nitrate, or a nutrient co-varying with it, and that the latter is controlled by the supply of nutrients from the pycnocline. These time series suggest that the system switches between distinct states characterized by high or low

phytoplankton biomass. The system may have switched to a low biomass state recently after a high biomass state during the previous 15 years.

5. Phytoplankton

5.1 Chl-a Concentration, Merged Sensors, Central and Southern California, 1996–2018

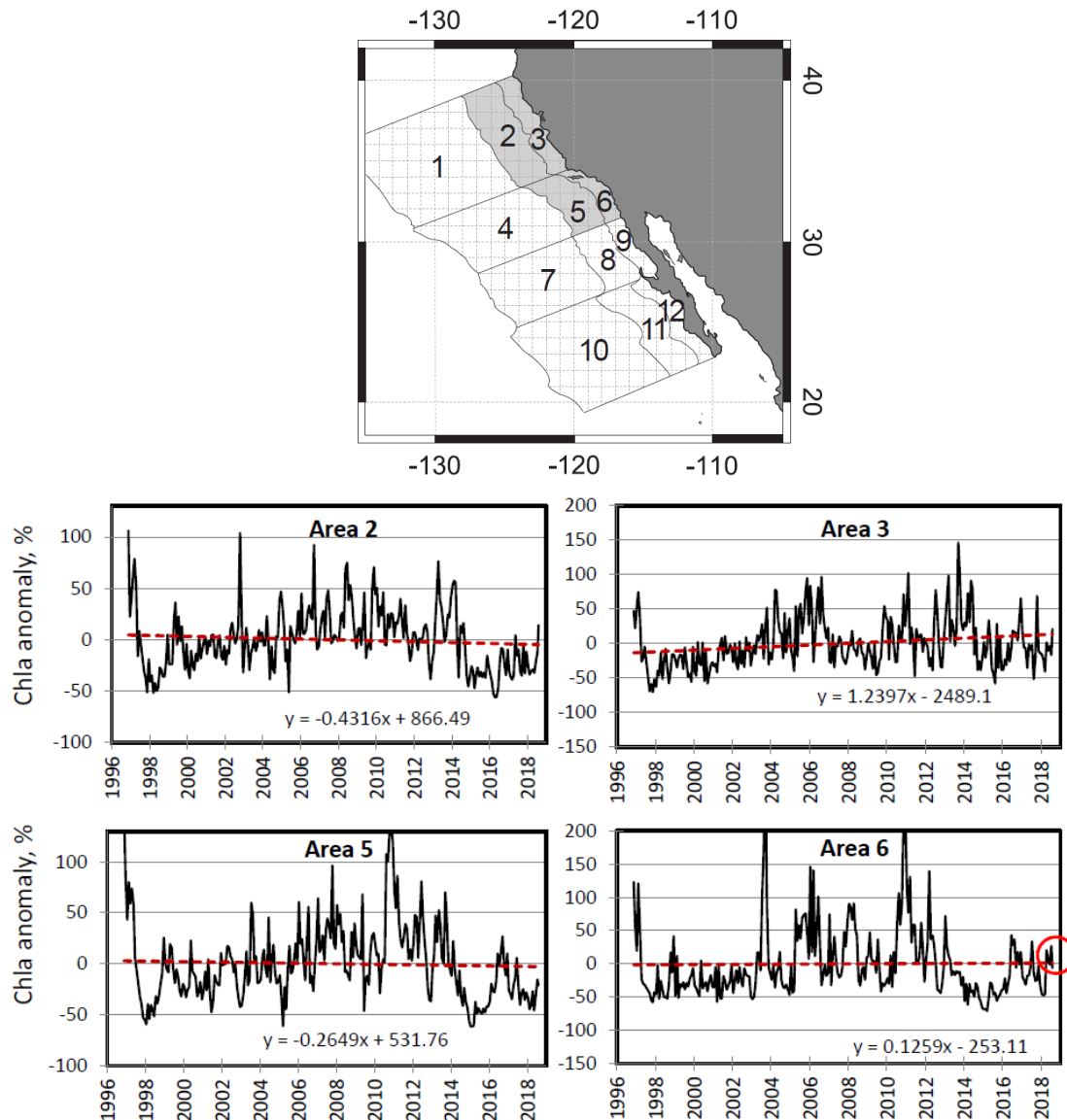


Figure R11-15. Time series of sea-surface chlorophyll-a concentration (chl-a) anomaly in the four areas. The data were derived from the merged multi-sensor regionally-optimized data set (Kahru et al. 2012, 2015, 2018).

Time series of sea-surface chlorophyll-a concentration (chl-a) were derived from the merged multi-sensor regionally-optimized data set (Kahru et al. 2012, 2015, 2018; <http://spg-satdata.ucsd.edu/CC4km/>). Monthly anomalies are calculated as ratios (expressed as %) relative to the long-term (1996–2018) monthly mean values. Time series are shown in four sub-areas: the coastal and transitional zones of central and southern California (Figure R11-15). After the period of high anomalies in 2014–2016 that in many areas resulted in all-time highest SST and lowest chl-a and minima in the frequency of surface fronts, the conditions in

2017 and the first half of 2018 returned to close to normal. While SST in 2017 was still slightly above the long-term average (by nearly 1 °C), by mid-2018 the SST values were close to the long-term means. In July–August, 2018, Southern California coastal waters experienced a positive SST anomaly of >2 °C but this anomaly covered only the coastal waters of the Southern California and northern Baja California regions. Chl-a values in 2017 and in the first half of 2018 were very close to normal in the coastal areas and slightly below the long-term means in the transitional areas. The positive SST anomaly in coastal Southern California did not have a strong effect on chl-a levels.

6. Zooplankton

6.1 Zooplankton Abundance, Baja California Pacific Coast, 1998–2018

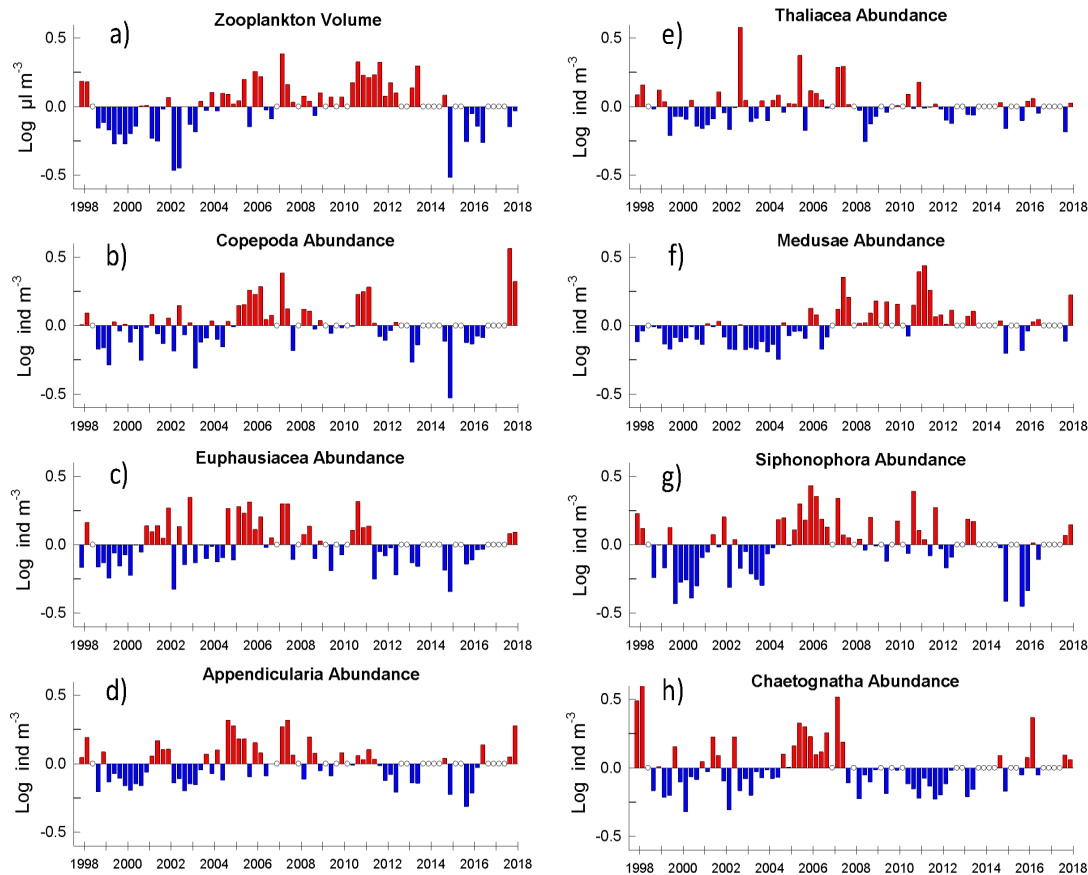


Figure R11-16. Timeseries of zooplankton abundance anomalies, Baja California Pacific Coast, 1998–2018.

Zooplankton is routinely sampled in the IMECOCAL cruises with oblique tows of a bongo net (500- μ m mesh width) from 210 m to the surface. In the laboratory, displacement volume is measured in all samples and zooplankton taxa are counted in a fraction of nighttime samples only. Zooplankton volume anomalies in the area between Ensenada and Vizcaino Bay, Baja California (lines 100 to 117), showed recovery after the 2014–2016 marine heat wave. In June 2017, zooplankton volume still showed negative anomalies but was of low magnitude, and after October 2017 the anomaly was close to zero (Figure R11-16a). The copepods zooplankton group experienced the highest increase in abundance during 2017 (Figure R11-16b), despite negative chlorophyll anomalies (Thompson et al. 2018). Euphausiid abundance anomalies were less impressive, showing a progressive recovery since the low levels observed in 2014 (Figure R11-16c). There was a delay in the recovery of gelatinous

herbivores. Appendicularians showed a substantial increase until October 2017 (Figure R11-16d), while thaliaceans had a negative anomaly in June 2017 (Figure R11-16e), mainly due to low abundance of salps and doliolids. Zooplankton carnivores presented two patterns, with medusae (Figure R11-16f) and siphonophores (Figure R11-16g) increasing mainly in October 2017 after low abundances during 2014–2016. In contrast, the chaetognaths showed a high positive anomaly in April 2016 and were slightly positive in 2017 (Figure R11-16h). In addition to the variable abundances in zooplankton groups, there were also changes in species composition. For example, euphausiid transition zone species as *Euphausia pacifica* and *Nematoscelis difficilis* decreased in 2014–2015 (Lavaniegos et al. 2019) and by October 2017 the rebound of these species was still incipient.

6.2 Zooplankton Abundance, Oregon, 1996–2018

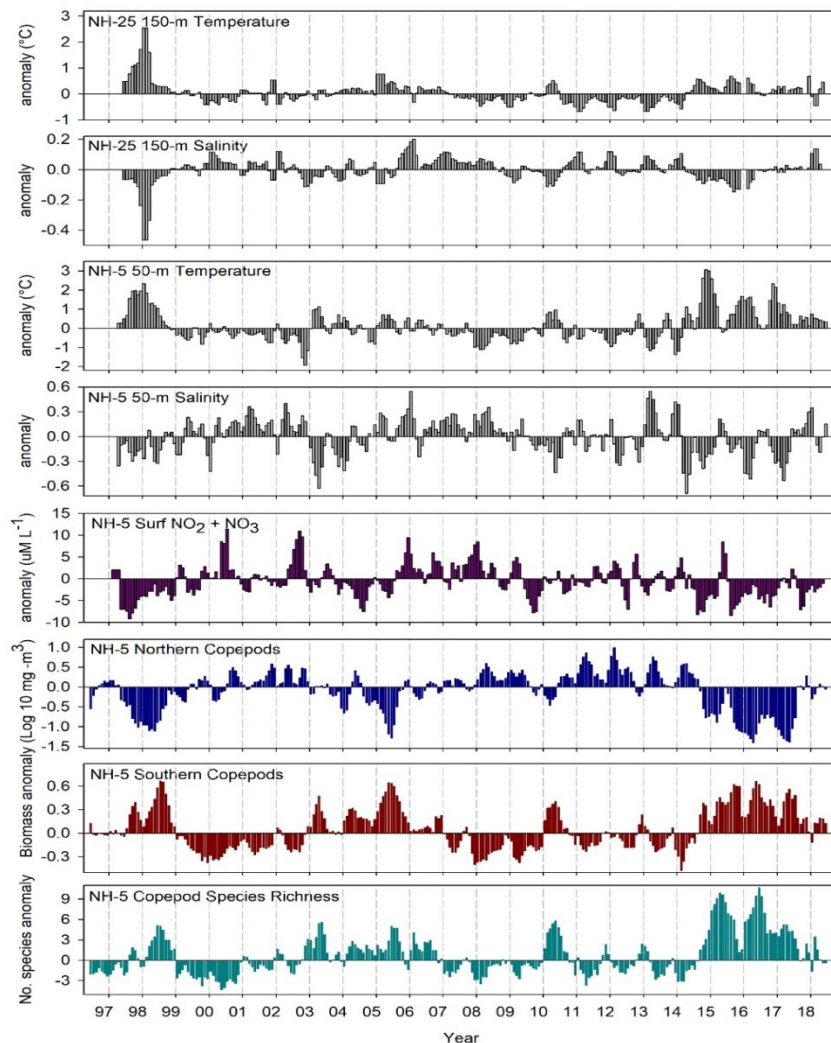


Figure R11-17. Zooplankton abundance, Oregon, 1996–2018.

Deep-water temperature anomalies on the slope and shelf off Newport, Oregon, were strongly positive from the spring of 2014 until summer 2017. These warm ocean conditions were associated with a lipid-depleted copepod community and a gelatinous-dominated zooplankton community, which persisted until summer 2017 when the copepod community transitioned to more a more neutral state (Figure R11-17; Peterson et al. 2017). During the period of strong temperature anomalies (fall 2014 until summer 2017), strongly positive anomalies of copepod species richness and southern copepod biomass were observed on the Oregon shelf, coupled with strongly negative anomalies of northern copepod biomass.

During the persistent upwelling season in 2017 (June–September), the positive temperature anomalies on the shelf and slope weakened and the strongly positive southern copepod biomass and species richness anomalies also weakened while the northern copepod biomass became neutral. During winter 2017–2018, species richness anomalies and the biomass anomalies of the northern copepods oscillated from weakly positive to weakly negative, while positive anomalies of southern copepods persisted. During 2015 and 2016, the copepod community did not transition from a warm-water winter copepod community to a cold-water summer community (data not shown). This ecologically important biological transition to a lipid-rich, cold-water community also did not occur in 1998, when warm ocean conditions occurred in the northern California Current (ENSO event). This transition did occur in June 2017, however, 52 days later than the 21-year average. In 2018 this biological transition occurred in late May, 22 days later than the climatology (data not shown). During the spring and summer of 2018, the shelf and slope waters were still warmer than average off Oregon and there was increased abundance of southern copepods on the shelf. Biomass of the northern copepods was more neutral, however, signaling that the pelagic ecosystem was in a state of flux between a warm copepod community and a cold upwelling community.

6.3 Diatom and Mesozooplankton Abundance and Copepod Size Structure, Southern British Columbia, 2000–2018: CPR survey

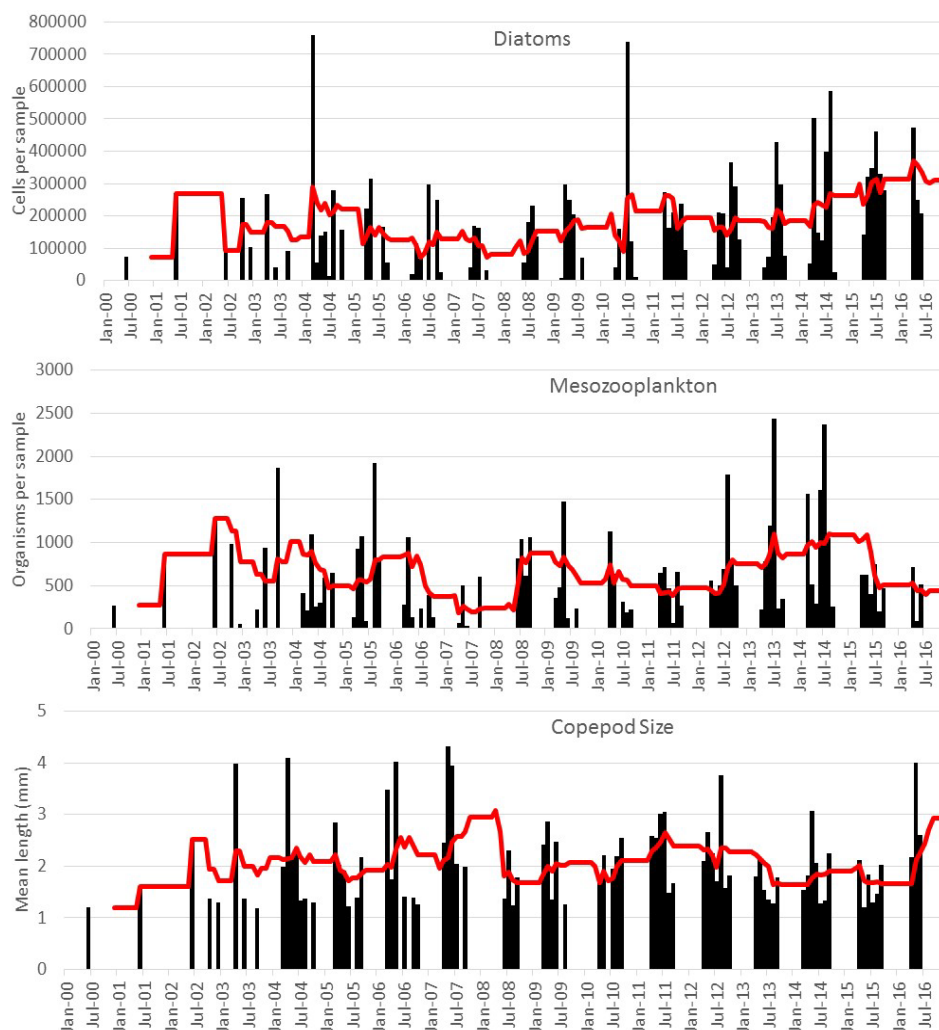


Figure R11-18. Diatom and mesozooplankton abundance and copepod size structure, Southern British Columbia, 2000–2018. Data were obtained by the Continuous Plankton Recorder survey.

The Continuous Plankton Recorder (CPR) is towed behind a commercial ship at a depth of about 7 m (see Figure R11-4d for the sampling area). The plankton are collected continuously and sectioned into 18.5-km samples (10 nautical miles) and normally every fourth sample is processed. Position, date, and time of the sample collection are taken from ship's log information and refer to the midpoint of the 18.5-km sample. Constant speed between log entries is assumed. Sampling began in 2000 and data are complete up to June 2016. Sampling begins each year in spring and in this region occurs approximately monthly until September/October. Three time series are shown in Figure R11-18. The first is total diatom abundance, which is the combined abundance of all diatom taxa recorded per sample. The second is mesozooplankton abundance, which is the combined abundance of all zooplankton taxa recorded per sample, with the exception of ciliates and eggs of copepods/euphausiids/fish. Note that all abundances given are 'per sample'. Theoretically, a sample is 3 m³ of filtered seawater, but this it isn't actually measured, and filtration efficiency can vary. The third is copepod size, where for each sample, the length L (mm) of each species i (adult female length), is multiplied by its abundance X_i , summed over all species N , and divided by the total abundance (Beaugrand et al. 2003). Data for all samples collected in the region each month were averaged to give a monthly mean, presented as black bars. The red line indicates a 12-month running mean to show long-term trends. There has been a general increase in large diatoms since 2008, although reasons why are not clear. Mesozooplankton abundance shows no long-term trend, but numbers declined from 2008 to 2011 before increasing again until 2015. The copepod size index shows larger taxa in 2008 and smaller taxa in 2013–2015, likely a response to the marine heat wave since warm conditions favour smaller, southern species.

6.4 Zooplankton Abundance, Southern British Columbia, 1990–2016: DFO Zooplankton Survey

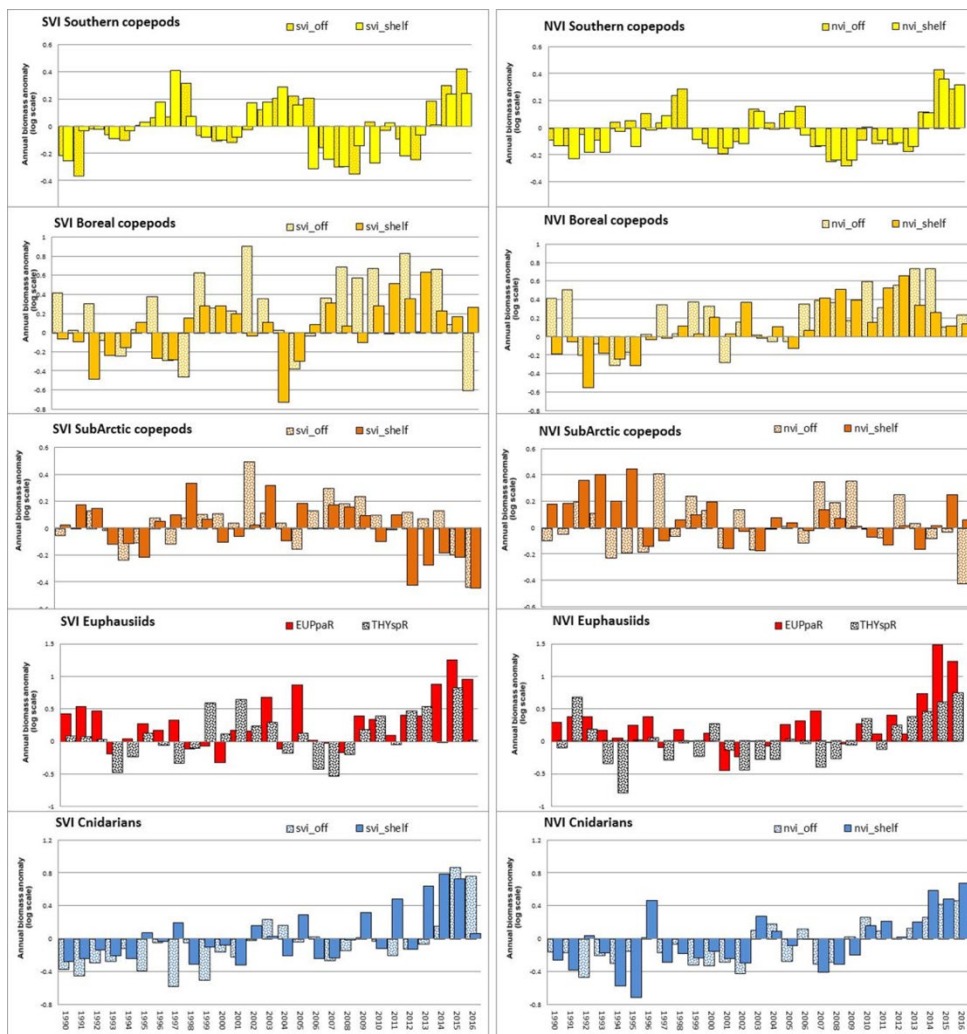


Figure R11-19. Zooplankton abundance, Southern British Columbia, 1990–2016. Data were obtained by Department of Fisheries and Oceans (DFO) Canada zooplankton survey

A clear, temporally-varying signal is evident in the three copepod groups (southern, boreal, and subarctic) and in the chaetognaths (Figure R11-19). Cool years such as the early 1980s, 1999–2002, and 2007–2009 have positive anomalies of boreal shelf and subarctic copepods and northern chaetognaths. Warm intervals such as 1983, 1993–1998, 2004–2005, and 2010 tended to have negative anomalies for these taxa, but positive anomalies in southern copepods and chaetognaths. Positive anomalies of the cool-water zooplankton community off Vancouver Island are associated with good local survival and growth of juvenile salmon, sablefish, and planktivorous seabirds (Mackas et al. 2007). Both southern and northern Vancouver Island nearshore and shelf regions had similar seasonal trends toward more southern copepods. The southern copepod signal was stronger in Hecate Strait (see Figure R11-4e for the sampling area) as these copepods are rarely transported that far north. The overall trend was negative for boreal and subarctic species for all of the west coast.

One of the main reasons for fewer boreal copepods is the almost near absence of *Pseudocalanus* species on the shelf in the south and the replacement of *Calanus marshallae*

with *Calanus pacificus* in the north. As in 2015, the 2016 influx of southern copepod species brought in some rarer animals not usually seen off the west coast except in large El Niño events: *Mecynocera clausi*, *Acartia tonsa*, *Acartia danae*, *Centropages bradyi*, *Clausocalanus mastigophorus*, *Aetideus giesbrechti*, *Pleuromamma gracilis*, *Pleuromamma indica*, *Paracalanus quasimodo*, *Parvocalanus crassirostris*, *Oithona tenuis*, *Rhincalanus nasutus*, and *Sapphirina* spp.

6.5 Variation in Length of *Euphausia Pacifica*, Northern California, 2007–2018

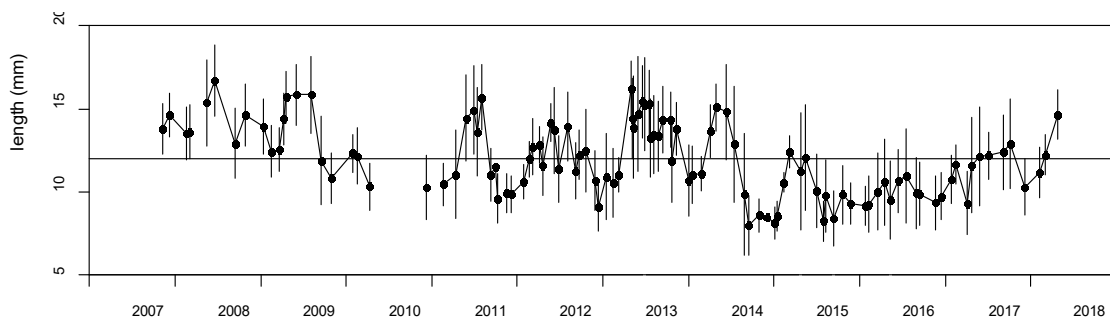


Figure R11-20. Variation in body length of *Euphausia pacifica*, Northern California, 2007–2018.

Over the last decade (late 2007 through mid-2018), ocean observing cruises have been conducted along the Trinidad Head Line (41.06°N) at roughly monthly intervals to collect hydrographic data and plankton samples representative of coastal waters off Northern California. Analysis of these data and samples focuses on characterizing the response of zooplankton assemblages and populations to local ocean conditions and larger-scale climate variation in support of coastwide ecosystem assessments (e.g., Bjorkstedt et al. 2011). Ongoing, more detailed analysis of these samples has revealed substantial seasonal and interannual variability in length of adult *Euphausia pacifica* and provides evidence that mean length is inversely related to temperature (Robertson and Bjorkstedt 2020). For example, during the 2014–2016 marine heat wave, mean lengths of adult *E. pacifica* were 15–20% lower than during the several preceding years (reductions in individual biomass were even more substantial). The smallest individual biomass and lowest mean lengths coincided with periods when waters of The Blob abutted the coast, and when the effects of the 2015–2016 El Niño manifested most strongly in the northern California Current. Such declines in individual size have potentially important consequences for foraging efficiency of krill predators—observed declines in euphausiid size are a possible contributing factor in concurrent seabird mortality events (Jones et al. 2018). In conjunction with temperature-associated shifts in euphausiid length, shifts in euphausiid assemblage structure have been linked to climate forcing (Robertson and Bjorkstedt 2020). For example, occurrences of “novel” warm water species such as *E. recurva* have been linked to the presence of water masses originating offshore (e.g., The Blob), while southern species (e.g., *Nyctiphanes simplex*) have occurred in association with strong poleward transport (e.g., the 2015–2016 El Niño). In contrast, cool water species declined in abundance: *Thysanoessa spinifera* effectively disappeared from our samples. Corroborating patterns are emerging from analyses of other zooplankton groups as well, supporting the hypotheses that advection plays a key role in shaping zooplankton assemblages off northern California, and confirming that, in general, shifts and trends in zooplankton assemblages observed off northern California are consistent with patterns observed elsewhere in the California Current, especially in the north.

7. Fishes and Invertebrates

7.1 Distribution and Abundance of Anchovy, Jack Mackerel, and Sardine Eggs: Continuous Fish-Egg Sampler (CUFES) survey, 2016–2018

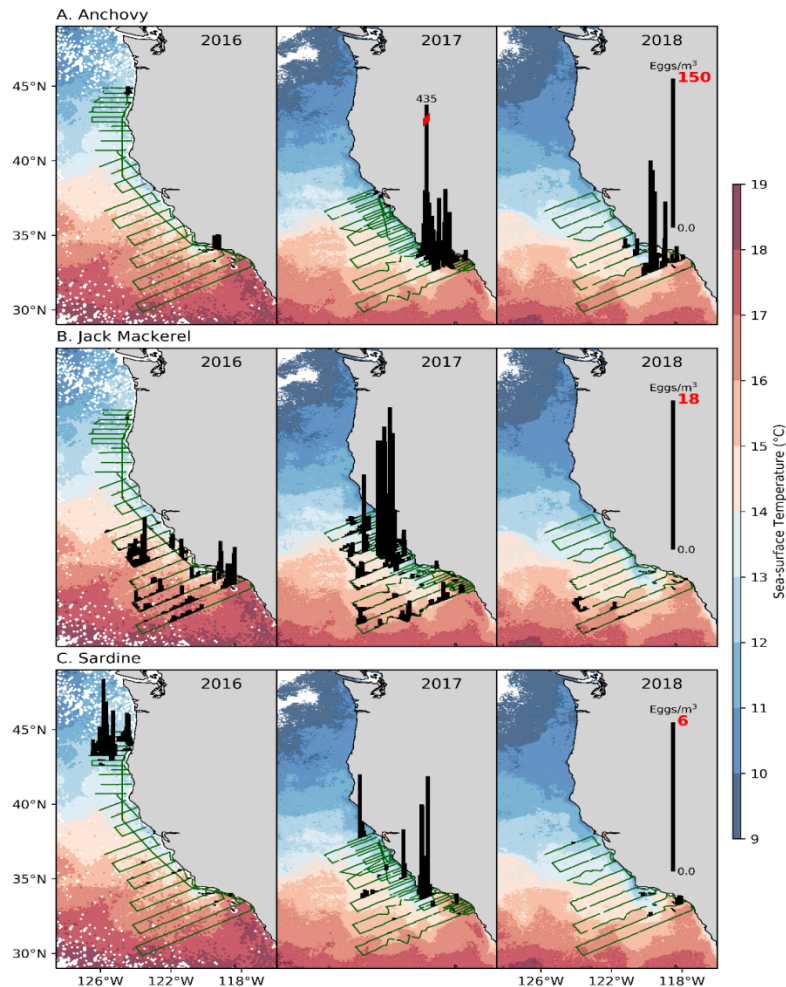


Figure R11-21. Distribution and abundance of anchovy (top), jack mackerel (middle), and sardine eggs (bottom), CUFES, 2016–2018. Data were obtained by the Continuous Fish-Egg Sampler (CUFES) survey.

CalCOFI collected data in the spring on coastal pelagic species (CPS) spawning from the ocean surface with a Continuous Fish-Egg Sampler (CUFES) and between the surface and 200 m with bongo nets (sampling methods are described in McClatchie (2014)). Both methods detected large increases in northern anchovy abundance in southern California in 2017 and 2018, which had been scarce in this region for the previous decade (Thayer et al. 2017) (Figure R11-21). Anchovy form an important forage base for many marine predators, and the improved condition of species such as California sea lions is probably directly caused by the anchovy surge (McClatchie et al. 2016). The rapid growth of the anchovy population was unexpected as there is a paradigm that anchovy thrive under cool conditions (Rykaczewski and Checkley Jr. 2008) and 2014–2016 were some of the warmest years on record in the California Current Large Marine Ecosystem (CCLME) (Jacox et al. 2018). This ecological surprise underscores the need to more fully develop mechanisms that affect anchovy recruitment (Checkley et al. 2017).

7.2 Abundance of Anchovy, Sardine, Jack and Pacific Mackerel Larvae, Southern California, 1950–2018

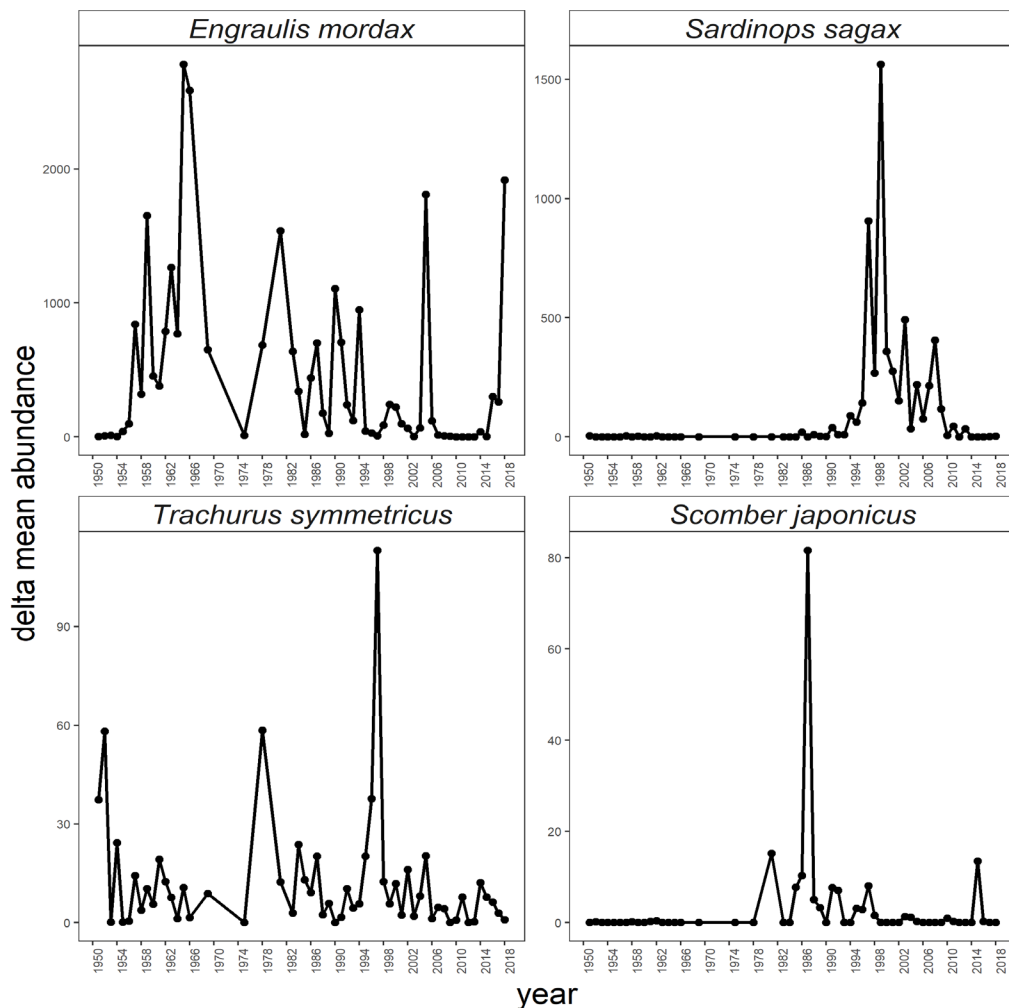


Figure R11-22. Larval abundance (number of individuals per haul) for anchovy (*Engraulis mordax*), sardine (*Sardinops sagax*), jack mackerel (*Trachurus symmetricus*) and Pacific mackerel (*Scomber japonicus*), Southern California, 1950–2018.

In contrast to anchovy larvae, Pacific sardine, jack mackerel, and Pacific mackerel larvae remained in low abundance in southern California in 2017–2018 (Figure R11-22), although jack mackerel were plentiful in central California in 2017. Pacific sardine have not been abundant in southern California since approximately 2008, and the combined scarcity of both anchovy and sardine likely stressed many marine predators including California sea lions (McClatchie et al. 2016). Although it has been hypothesized that sardine do well when conditions are warm, this was apparently not borne out following the 2014–2016 warm period.

7.3 Biomass of Larval Forage Fishes, Oregon and Washington, 1998–2018

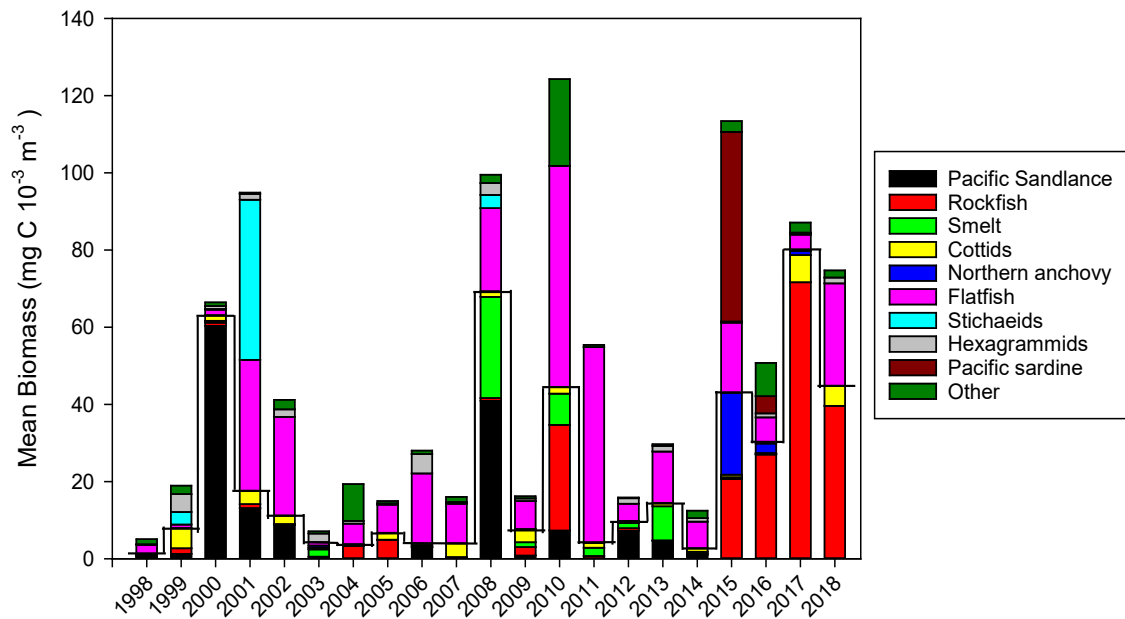


Figure R11-23. Annual mean biomass ($\text{mg C } 1000 \text{ m}^{-3}$) of larvae of the five important salmon prey taxa (below solid line) and five other dominant larval fish taxa (above solid line) collected during winter (January–March) in 1998–2018 along the Newport Hydrographic (NH) line off the coast of Oregon ($44^{\circ}65' \text{ N}$, $124.18\text{--}124^{\circ}65' \text{ W}$).

The biomass of fish larvae in winter (January–March) derived from the Newport Hydrographic line provides an index of fish that are the common prey of sea birds and juvenile salmon entering the ocean in spring and summer (Gladics et al. 2014, Daly et al. 2017). When ichthyoplankton biomass was high in winter, such as in 2001 or 2008 (Figure R11-23), common murre reproductive success was higher and salmon smolt-to-adult returns were higher later in the year. When fish larval biomass was low, such as in 1998 or 2012, food conditions were poor and therefore seabird reproductive success and salmon returns were also correspondingly low. Since 2015, winter fish larvae biomass has been high but was generally comprised of offshore taxa indicative of warm ocean conditions (rockfishes [*Sebastes* spp.] and northern anchovy [*Engraulis mordax*]; Auth et al. 2018).

7.4 Abundance of Juvenile Rockfish and Associated Species, California, 1990–2018

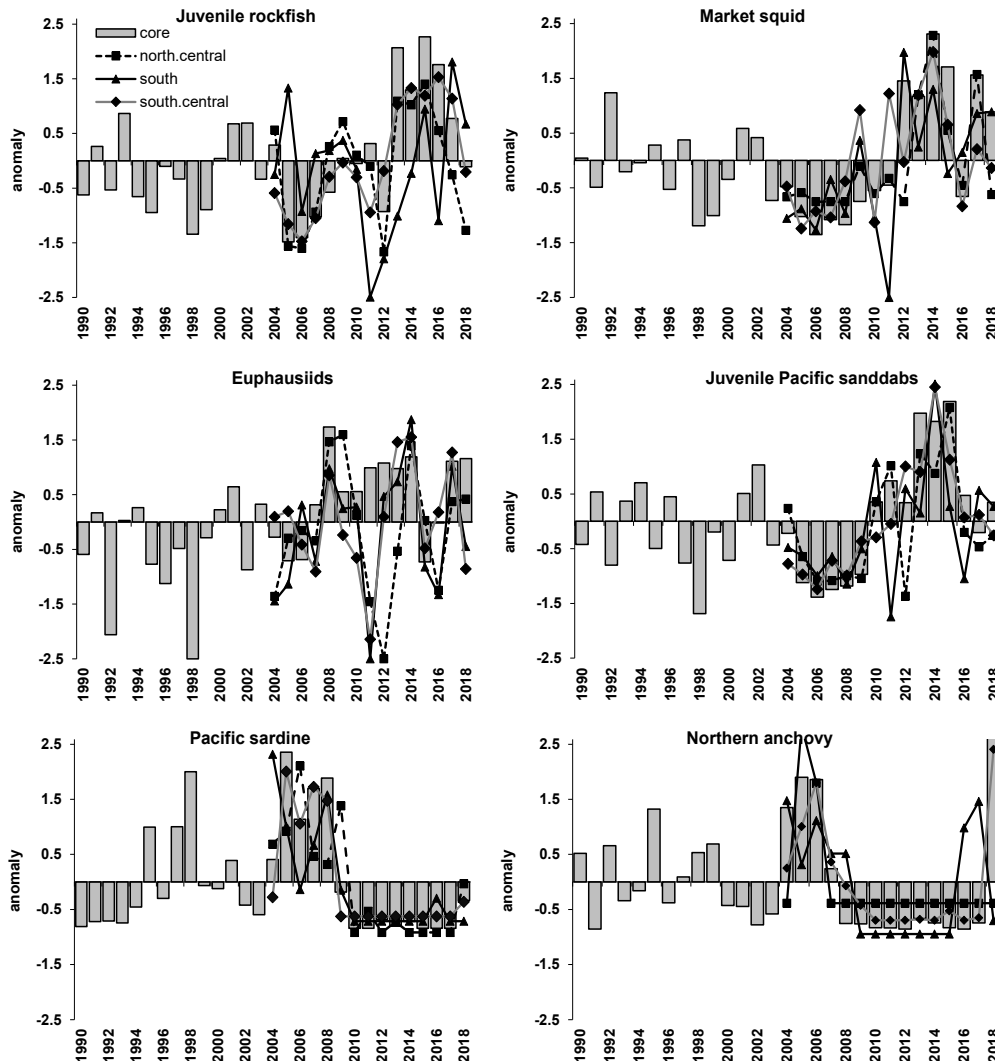


Figure R11-24. Standardized anomalies of average ($\ln(\text{catch}+1)$) catches for key forage taxa (adult) sampled by the Rockfish Recruitment and Ecosystem Assessment Survey.

Catches of juvenile groundfish and epipelagic micronekton from the Rockfish Recruitment and Ecosystem Assessment Survey (Sakuma et al. 2016; see the survey area in Figure R11-4b) in late spring of 2018 indicated declines from the high abundance levels during 2015–2017 for pelagic young-of-the-year (YOY) rockfish (*Sebastes* spp.) and sanddabs (*Citharichthys* spp.) throughout most regions off California (Figure R11-24). The exception was fairly high YOY rockfish abundance in the southern California Bight. There was a significant increase in the abundance of adult northern anchovy (*Engraulis mordax*) in the core and south central regions in 2018 and their abundance was at its highest since 2005–2006. A small number of adult Pacific sardine (*Sardinops sagax*) were encountered, more than in roughly the last ten years, but still very low relative to the high abundance levels in the late 1990s and early 2000s. YOY northern anchovy and Pacific sardine (not shown) were also at relatively high levels in the survey, particularly in the southern survey region. Market squid (*Doryteuthis opalescens*) and krill (euphausiids) were at fairly high abundance levels in most regions, particularly in the core and Southern California Bight. Pelagic red crabs

(*Pleuroncodes planipes*, not shown) were also at high abundance levels in the southern California Bight during the late spring of 2018, a phenomenon sustained since 2015.

7.5 Abundance of Juvenile Coho and Chinook Salmon, Oregon and Washington, 1998–2018 (Figure R11-25)

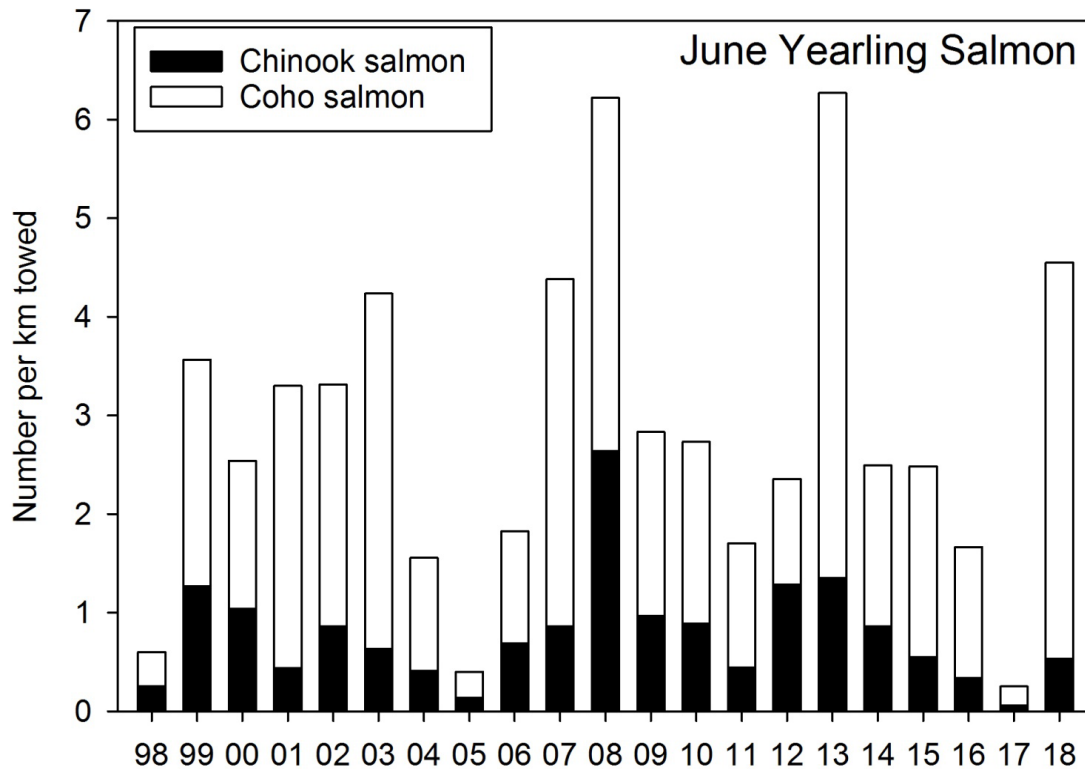


Figure R11-25. Abundance (number km⁻¹) of juvenile Coho and Chinook salmon, Oregon and Washington, 1998–2018. Data were obtained by the Northwest Fisheries Science Center (NWFSC).

This survey has been conducted by the Northwest Fisheries Science Center (NWFSC) in late June every year between 1998 and 2018. Sampling occurred along 11 east–west transect lines off Washington and Oregon, ranging from approximately 45° to 48°N. Trawls were conducted at 6–8 stations on each transect from the shallowest bottom depth possible (~30 m) out to ~50 km from shore, often extending beyond the continental shelf (Brodeur et al. 2005, Peterson et al. 2010). Sampling was conducted during daytime in the upper 20 m of the water column at every station using a pelagic rope trawl with the head rope at about 1 m and a 336 m² mouth opening with variable mesh sizes (162.6 cm at mouth to 8.9 cm at cod end). To retain catches of small nekton, a 6.1 m long, 0.8-cm mesh knotless liner was sewn into the cod end. The rope trawl was towed for 30 minutes at a speed over ground of approximately 6 km h⁻¹. Catches of yearling salmon off Washington and Oregon in June are thought to be accurate indicators of early ocean survival of yearling Chinook and Coho salmon. The abundance of yearling Chinook salmon during June surveys has a significant, positive relationship to returning spring Chinook jack and adult salmon counts at Bonneville Dam on the Columbia River (with 1- and 2-year lags, respectively), as does the abundance of yearling Coho salmon to subsequent Coho smolt to adult survival (Morgan et al. 2018). Catch per unit effort (CPUE, number per km trawled) of both yearling Chinook and Coho salmon during the June 2017 survey was the lowest of the 20-year time series from 1998 to 2017 (Figure R11-25). In June of 2018, yearling Chinook salmon catches were slightly below average, but yearling Coho salmon catches were the second highest in the 21-year

time series (Figure R11-25). Based on correlations observed in previous years, this suggests that adult returns of spring Chinook salmon in 2020 will be close to average and adult Coho salmon returns in 2019 will be higher than average.

7.6 Select Fisheries Landings, 1970–2018 (Figure R11-26)

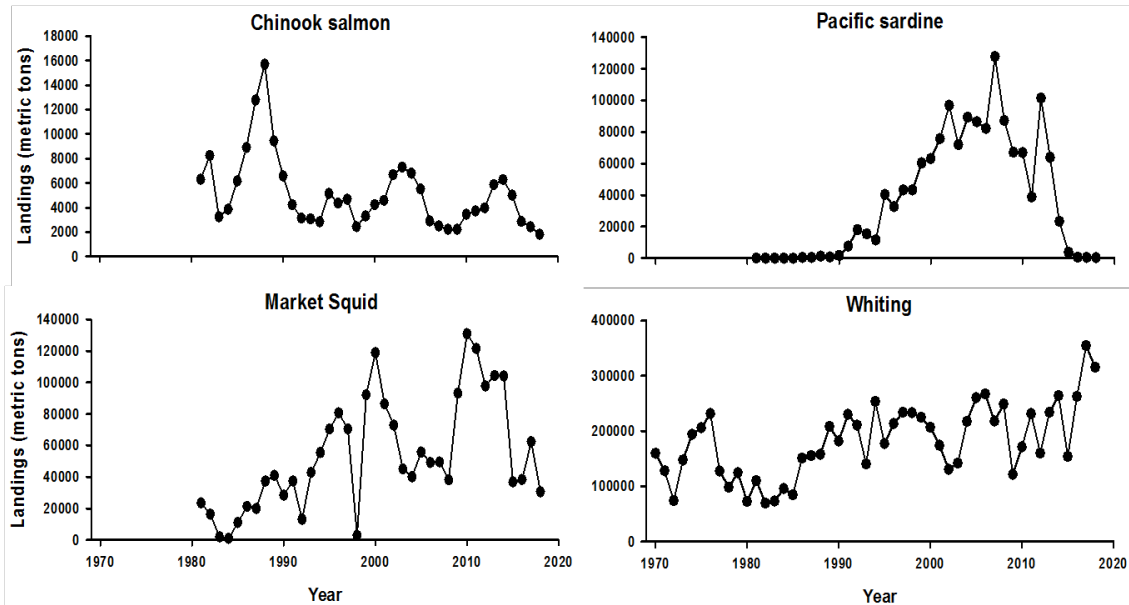


Figure R11-26. Select fisheries landings, 1970–2018. Data were obtained from the Pacific Fisheries Information Network (PacFIN) and reflect landings across the California Current.

Chinook salmon landings were at a peak of ~16,000 metric tons (MT) in 1988, but catch in most years has been between 2000–7000 MT. Landings also appear to have occurred in a cyclical manner and display a slight decreasing trend over the course of the time series. Landings of Pacific sardine show an increase followed by a decrease over the time series. There were very few landings until the late 1980s. Catch increased and peaked at approximately ~128,000 MT in 2007, then decreased very quickly. Only a few hundred MT of sardine were caught since 2016. Catch of market squid shows a slight increasing trend over the time series, though with a couple periods of lower catch. Landings were particularly low in 1983–84 and 1998, all years of El Niño warm water events. Once landings increased in the 1990s, other periods with fewer landings were 2003–2008 and 2015–2018. Peak catch was in 2010 at ~130,000 MT. Whiting landings also have a steady increasing trend over the time series. Landings were always greater than ~70,000 MT, and peaked in 2017 at ~354,000 MT. Data were provided by the Pacific Fisheries Information Network (PacFIN), retrieval dated February 27, 2019, Pacific States Marine Fisheries Commission, Portland, Oregon (www.psmfc.org).

8. Marine Birds

8.1 Variation in Seabird Breeding Success, Central California, 1971–2018 (Figure R11-27)

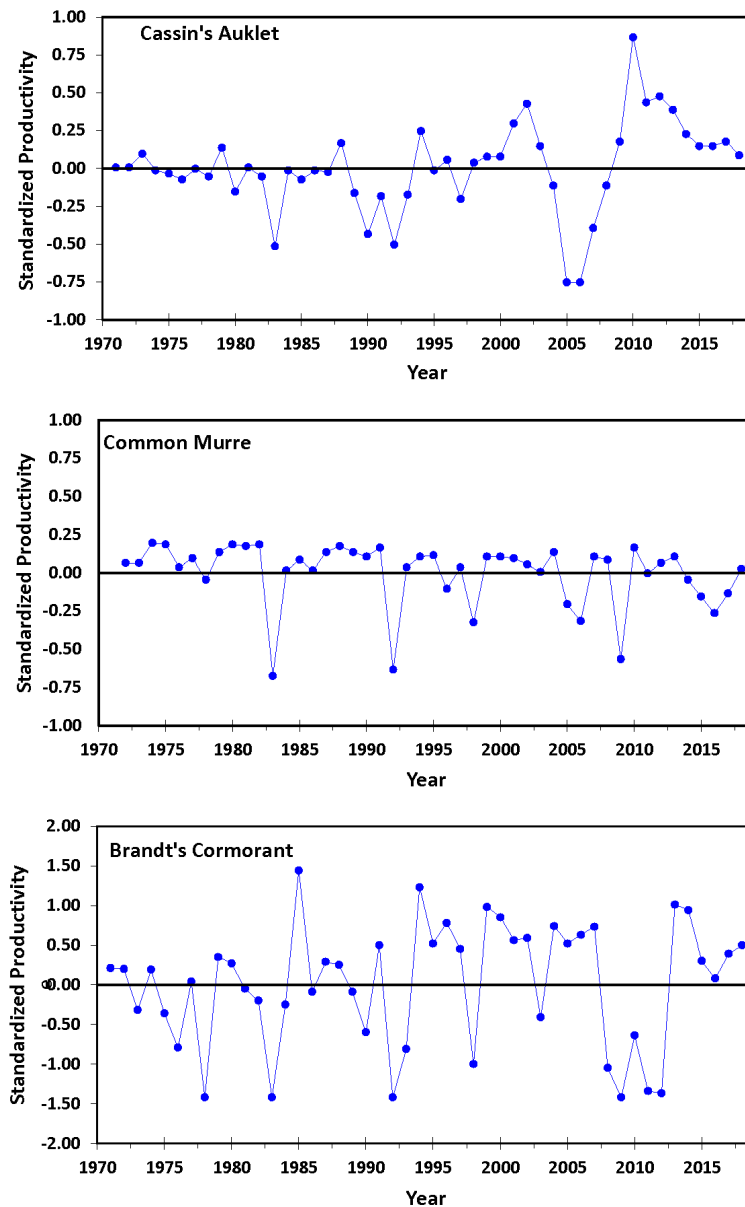


Figure R11-27. Variation in productivity for 3 species of seabird breeding on Southeast Farallon Island, central California, 1971–2018.

The data shown above are standardized productivity anomalies (annual productivity minus the 1971–2018 mean) for Cassin's auklet (*Ptychoramphus aleuticus*), common murre (*Uria aalge*), and Brandt's cormorant (*Phalacrocorax penicillatus*) on SE Farallon Island. In the last decade, Cassin's auklet productivity has recovered following the breeding failures of 2005 and 2006, reaching a peak in 2010. Productivity has declined since then but remains just above normal. Common murre productivity suffers occasional lows. The last year of

severe low productivity was 2009, though it was also lower than average in 2015–2017, presumably corresponding to effects from the marine heat wave (with a slight lag). Other years in the last decade have been near average. Brandt’s cormorant productivity is variable on the interannual scale. Productivity was low through from 2008–2012, with very low values in 2009, 2011, and 2012. They recovered in 2013, however, with fairly high productivity in that year and also 2014. Since then, productivity has been closer to normal, but above average

8.2 Variation in Seabird Breeding Success, Oregon, 1998–2017

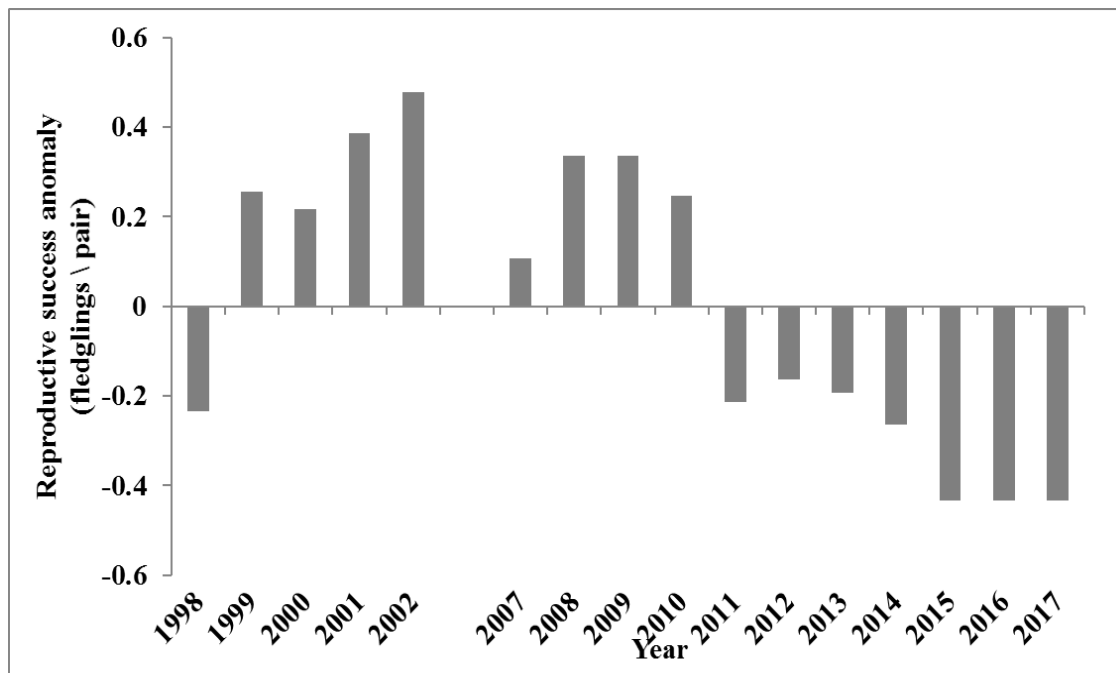


Figure R11-28. Productivity of the most common seabird in Oregon, common murre (*Uria aalge*), 1998–2017.

Common murre (*Uria aalge*) reproductive success was measured at Yaquina Head (R11-4b), OR, from 1998–2017, with a gap in the time series from 2003–2006 (Figure R11-28). The Yaquina Head Outstanding Natural Area is home to some of Oregon’s largest and most publically visible seabird colonies, including over 60,000 seabirds. Yaquina Head (44.68°N, 124.08°W) is also located in one of the most intensely studied portions of the northern California Current System. The study site is adjacent to the Newport Hydrographic Line (25-year time series) and the Endurance Array cabled ocean observatory (NSF OOI, in second year of operation). Seabird data at Yaquina Head are collected during the summer upwelling period and have shown strong correlation with indices of local-scale biological productivity (e.g., winter ichthyoplankton biomass, summer northern copepod biomass), as well as local- (upwelling index) and basin-scale physical (PDO, NPGO) processes (Gladics et al. 2015). Murres are deep diving (≤ 170 m), piscivorous (primarily) predators capable of foraging throughout the water column on the continental shelf, but will extend their foraging range offshore beyond the shelf break during the breeding season. Reproductive success increased from 1998–2002 and dramatically declined from 2008–2017, culminating in reproductive failure (0% productivity) in 2015–2017. Productivity was also low in 1998, perhaps due to effects of the 1997–1998 El Niño event. Since 2011, reduced reproductive success has been caused by predation by bald eagles, which preyed upon chicks and eggs. Eventually this predation was lessened due to the diminishing numbers of eggs available, but presence of the eagles also prevented murres from attempting to breed. Additionally,

there was evidence that food conditions for breeding murres in those later years were poor. Our studies also document the influence of recovering predator populations and provide insight into the relative importance of bottom-up vs. top-down forcing as predator populations recover and reoccupy their historical ranges (Horton 2014). Seabird studies at Yaquina Head provide an important contribution to understanding local, upper-trophic level biological impacts of North Pacific climate fluctuations.

8.3 Abundance of Seabirds at Sea, Southern California, 1987–2018

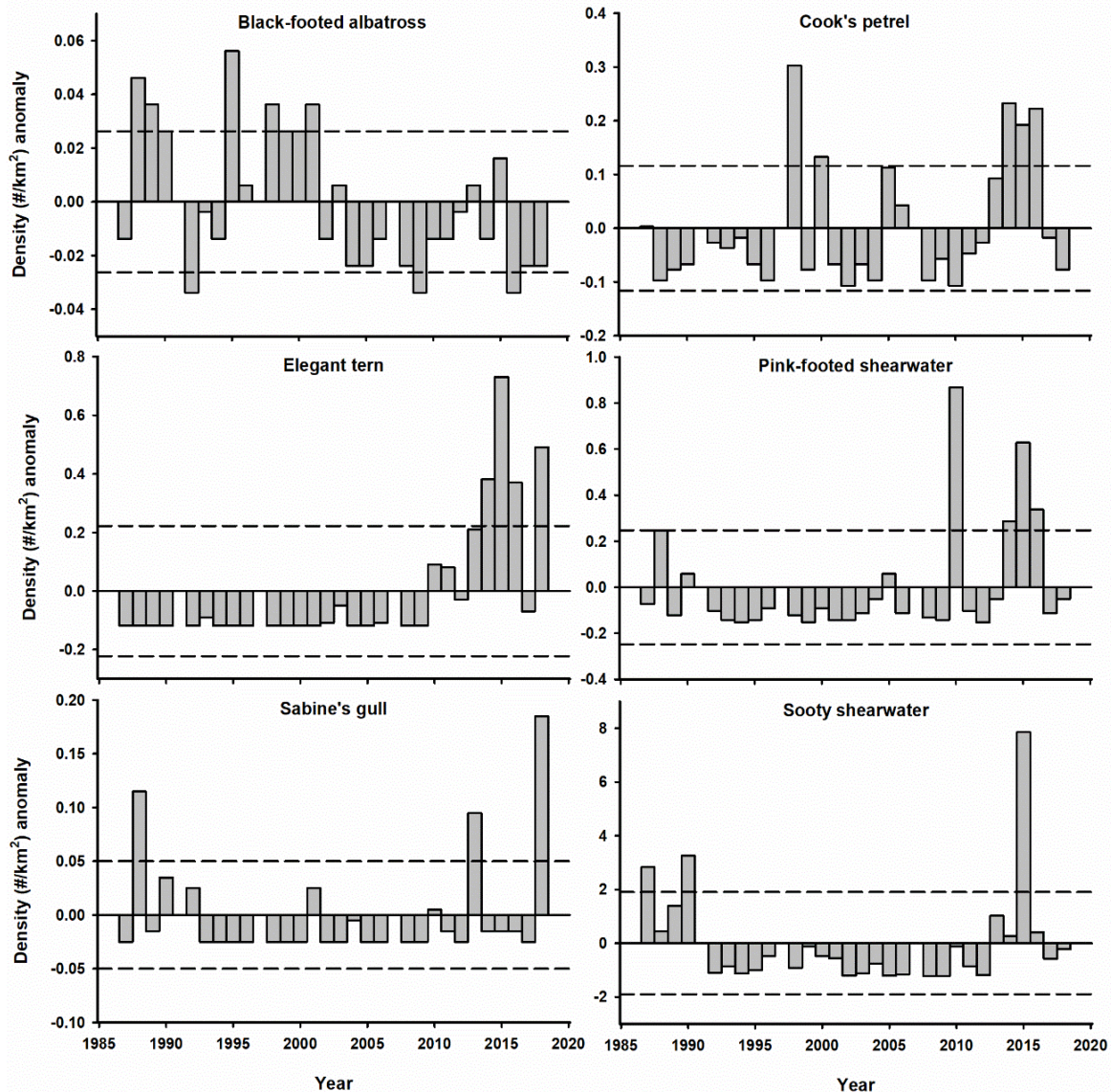


Figure R11-29. Population trends of 6 species of seabird off Southern California, based on springtime CalCOFI surveys. Data provided courtesy Farallon Institute.

Figure R11-29 shows seabird density at sea on the spring CalCOFI surveys (R11-4a), 1987–2018. An observer aboard the ship records observations of all individuals seen within a 300-m strip transect to one side and front of the vessel while the ship is underway at <5 knots (Hyrenbach and Veit 2003). Here, we present results for six seabird species: black-footed albatross (*Phoebastria nigripes*), Cook's petrel (*Pterodroma cookii*), elegant tern (*Sterna elegans*), pink-footed shearwater (*Puffinus creatopus*), Sabine's gull (*Larus sabini*), and sooty shearwater (*Ardenna griseus*). Black-footed albatross show a general decreasing trend over the course of the time series with higher than average density prior to 2002, and

lower densities since then. The low density in 2018 marked the third consecutive year for density at or near -1 s.d. Cook’s petrel are present in occasional high abundances during this survey, and they had high density in the period 2013–2016. Elegant tern has mostly not been present during this survey, but their density has increased steadily since 2010. There is evidence that elegant terns are experiencing a range expansion northward in southern California (Velarde et al. 2015) and our data support these observations. Pink-footed shearwaters are also present in occasional high abundances, with the most recent period of high density being 2014–2016. In 2018, there was the highest ever recorded density of Sabine’s gull in the spring survey. This species is not typically abundant during this survey, but there are occasional years of high density. Sooty shearwaters were present at the beginning of the time series until 1990, then were present in low abundances during this survey until recently. There was a tremendous spike in there abundance in 2015 and since then they have been present at near-average numbers.

8.4 Seabird Mortality Event

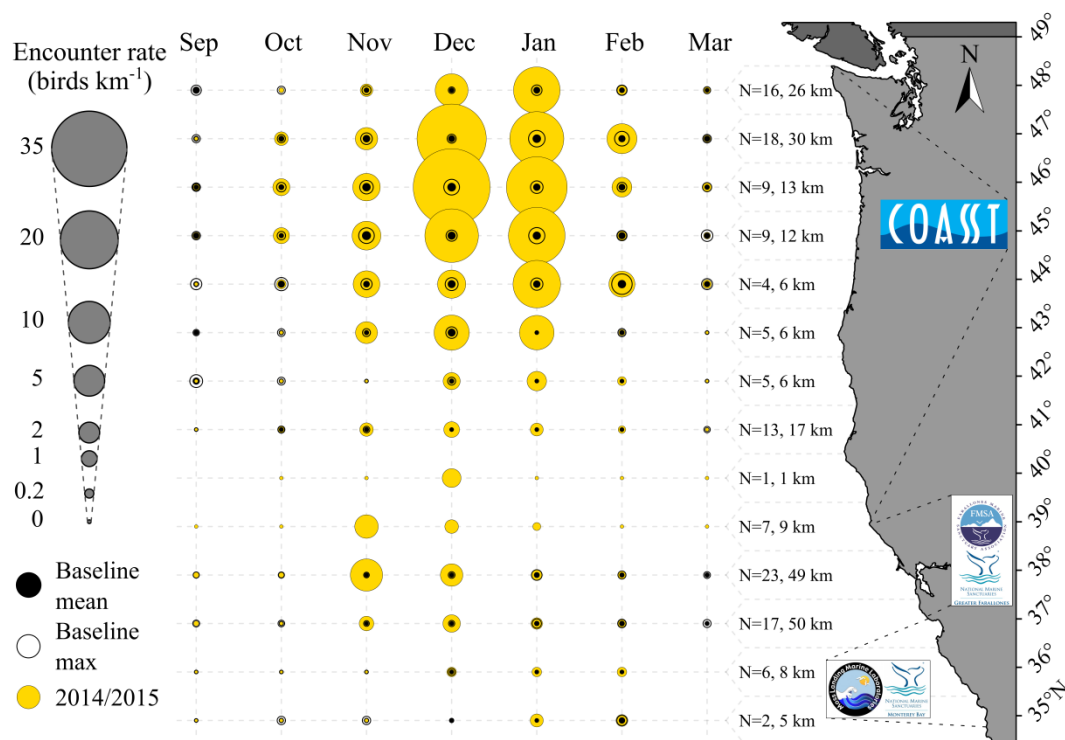


Figure R11-30. The 2014/15 winter mortality event of Cassin's auklets. N: average number of beach segments surveyed, km: distance surveyed throughout each time period.

The 2014/15 winter mortality event of Cassin's auklets (*Ptychoramphus aleuticus*) and other small alcids (1% ancient murrelets, *Synthliboramphus antiquus*; 0.5% marbled murrelets, *Brachyramphus marmoratus*; and 0.1% Scripps's murrelets, *Synthliboramphus scrippsi*) was observed. Figure R11-30 shows monthly-averaged encounter rate (carcasses per km of beach surveyed) within 0.5-deg latitude segments of coastline from September 2014 to March 2015 in comparison to long-term baselines from three beached bird programs: COASST (N. California north to WA), BeachWatch (N. California south to Monterey Bay), and BeachCOMBERS (south of Monterey Bay). Sample sizes (N) refer to the average number of beach segments and distance (km) surveyed throughout each time period. Cassin’s auklets, a small zooplanktivorous seabird, were found in unprecedented high mortality over a 3–4 month period following the onset of the northeast Pacific marine heat wave in 2014–2016. Widespread mortality followed documented shifts in zooplankton composition, including declines in abundance of large lipid-rich copepods and euphausiids,

and an increased abundance of small sub-tropical copepod species (R11-17). Shifts in prey composition were coincident with the loss of cold-water foraging habitat caused by the intrusion of the marine heat wave into the nearshore environment in the late fall of 2014. Models examining interannual variability in effort-controlled carcass abundance (2001–2014) identified the biomass of lipid-poor zooplankton as the dominant predictor of increased carcass abundance for Cassin's auklets even with the untoward 2014 event removed, suggesting a causal link between prey quality and post-breeding survival. Collectively these results suggest that in 2014, Cassin's auklets dispersing from colonies in British Columbia likely congregated into a nearshore band of cooler upwelled water, and ultimately died from starvation following the shift in zooplankton community composition associated with onshore transport of the NE Pacific marine heat wave. This event represents one of several seabird mass mortality events that have occurred in the North Pacific over the last five years.

9. Marine Mammals

9.1 Variation in California Sea Lion Production, Southern California, 1997–2017

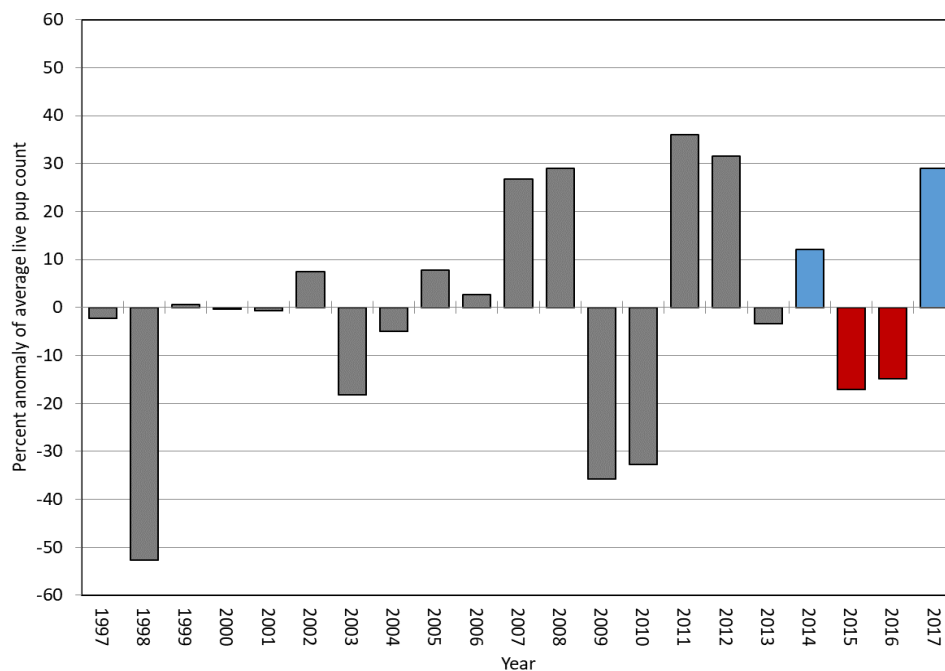


Figure R11-31. Variation in production (percent anomaly of average live pup count) at the San Miguel sea lion colony.

Between 1997 and 2017, live California sea lion pups were counted at San Miguel Island, California (34.03°N, 120.4°W) as measure of successful births and as an indicator of prey availability to and nutritional status of nursing females from October to the following June. The San Miguel sea lion colony represents about 45% of the U.S. breeding population and is a useful colony to measure trends and population responses to changes in the marine environment. Each July, live pups were counted after all pups were born. A mean of the number of live pups was calculated from the total number of live pups counted by each observer. A long-term average live pup count based on counts between 1997 and 2017 was used to create annual anomaly percentages from the long-term average (Figure R11-31). The annual number of California sea lion pup births has been quite variable since 2009 owing to several regional marine events that altered the availability of prey to pregnant and nursing females, the strongest of which were the 2009 upwelling relaxation event and 2010

El Niño conditions. However, the marine heat wave resulted in a significant decline (26%) in the number of live California sea lion pups between 2014 and 2015. The live pup census in 2016 showed some improvement with the number of pups increasing 3% from 2015 to 2016, however it was still 15% below the time series average (Figure R11-31). In 2017, the number of live pups increased 52% from 2016 and exceeded the long-term average by 29%. The return of births to the long-term average in 2017 indicates that the lower number of births in 2015 and 2016 were not simply the result of fewer reproductive females in the population but that due to the poor foraging conditions during the gestation period, when fewer reproductive females were able to energetically support pregnancies. The return of cooler ocean conditions and more normal oceanographic patterns along the central California coast in early 2016 and throughout 2017 contributed to the return of anchovy to the prey community (Figure R11-22 & 23) and to the diet of nursing females, which coincided with an increase in pup births in 2017.

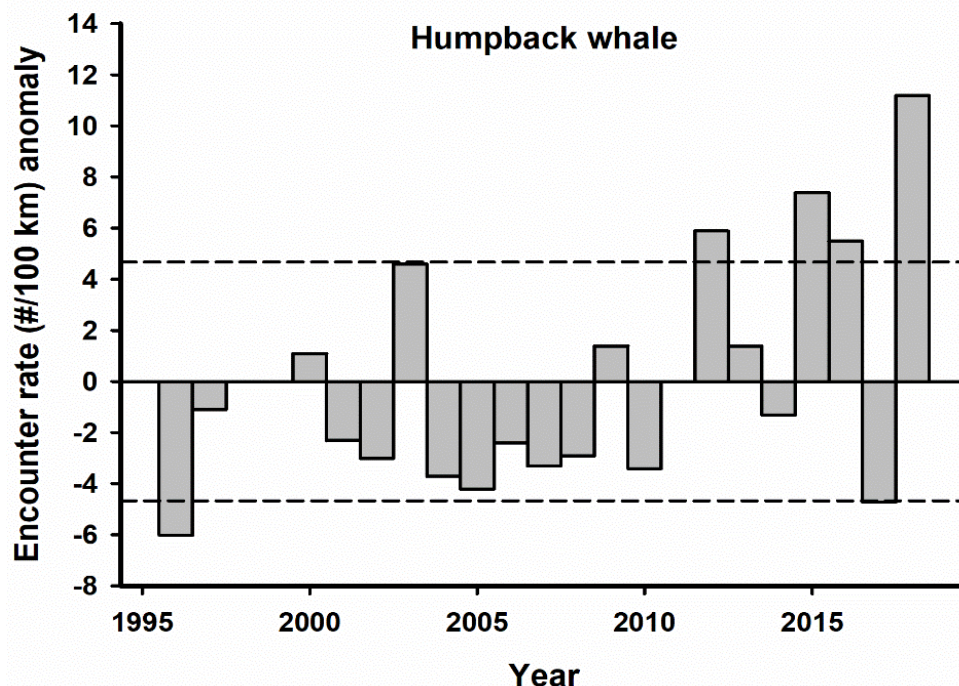


Figure R11-32. Population trends of humpback whale in central California based marine mammal observations conducted by Farallon Institute on the annual Rockfish Recruitment and Ecosystem Assessment Survey (RREAS).

9.2 Variation in Humpback Whale Abundance, Central California, 1996–2018

This figure shows anomalies of humpback whale observations (*Megaptera novaeangliae*; 1996–2018) on the NOAA Rockfish Recruitment and Ecosystem Assessment Survey, which takes place each spring/summer offshore of Central California (Figure 11R-4b). An observer on the ship records all observations of humpback whales out to the horizon on one side of the ship while it's underway. Abundance is expressed as an encounter rate (#/100 km). The time series shows an increasing trend in encounter rate, though there were fewer seen in 2017. In 2018, on the other hand, there was the highest number of humpback whale observations in the history of this survey.

10. Pollutants/Contaminants

10.1 Marine Debris Types, 2012–2016

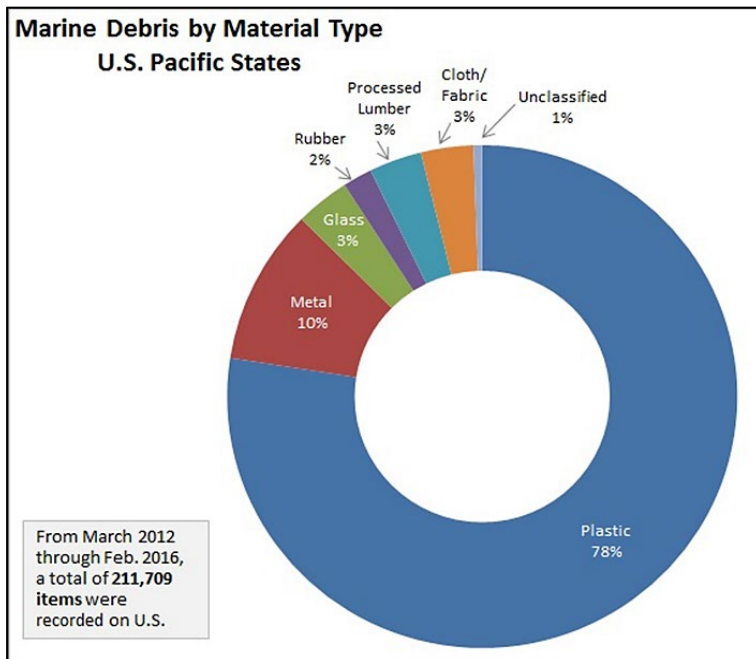


Figure R11-33. Marine debris types observed along the U.S. Pacific states shorelines, 2012–2016, based on the NOAA Marine Debris Monitoring and Assessment Project (MDMAP).

The NOAA Marine Debris Monitoring and Assessment Project (MDMAP) is a citizen science initiative that engages NOAA partners and volunteers across the nation to survey and record the amount and types of marine debris on shorelines. Across all MDMAP surveys in U.S. Pacific states (Alaska, Washington, Oregon, California, and Hawaii), 211,709 debris items were recorded between March 2012 and February 2016. Plastic debris items comprised 78% of the debris recorded (Figure R11-33). Of the plastic items recorded, hard, foamed, and filmed plastic fragments dominated, accounting for 54% of the total (a fragment is a piece of a larger item that cannot be identified). Identifiable items that appear in the top ten list across all states include plastic rope/small net pieces, bottle/container caps, food wrappers, and plastic beverage bottles. Notably, bottle/container caps are in the top four most common items in all states. The MDMAP data indicate that in Alaska, California, and Oregon, plastic consumer items are at least twice as common as plastic fishing-related items. In Hawaii, plastic fishing-related products are slightly more common than plastic consumer items, whereas in Washington there is about an equal split between the two user categories. The results of long-term marine debris monitoring studies, particularly the most abundant items and likely sources, can be applied to policy development, education, and outreach, and research initiatives at various spatial scales. Given increasing interest in addressing marine debris from local municipalities to the international stage, programs such as MDMAP are essential for scientifically documenting the issue, monitoring change, and tracking progress.

10.2 Poly-aromatic Hydrocarbon Concentration in Blue Mussels, 1989–2012

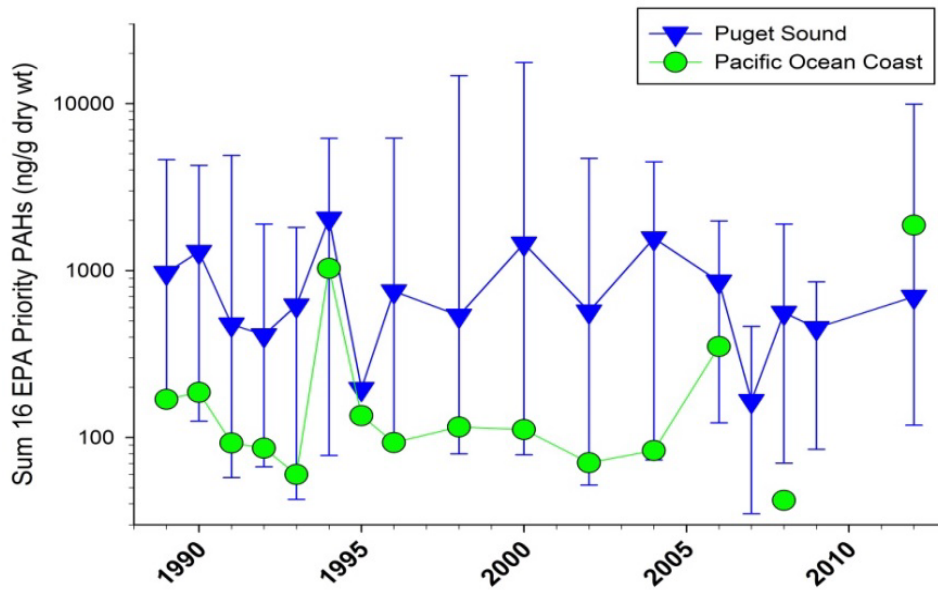


Figure R11-34. Poly-aromatic hydrocarbon concentration in blue mussels in inland marine waters of Washington State, based on the NOAA's Mussel Watch Program (MWP), 1989–2012.

Polycyclic aromatic hydrocarbons (PAHs), a class of chemicals found in petroleum products spilled into the environment and/or released into the air when fossil fuels and wood or grass are burned, represent one of the most common and abundant groups of toxic contaminants in U.S. coastal marine waters. Many PAHs are highly toxic to fishes and invertebrates, especially to developing fish embryos. NOAA's Mussel Watch Program (MWP) tracks PAHs and other chemicals in coastal marine bivalves (mussels and oysters) to observe spatial and temporal trends in chemical pollutants on a national scale (Kimbrough et al. 2008). MWP sampling in Washington State consisted of biennial collections of wild mussels from approximately 25 locations along Washington's inland marine waters (Puget Sound and the Salish Sea) and the Pacific coast shoreline from 1989–2012. Over the decades the concentrations of PAHs in Puget Sound mussels remained consistent and relatively high compared to the Pacific coast (Mearns 2001) (Figure R11-34). Overall, Puget Sound mussels had roughly 5 times the amount of PAHs than coastal mussels. More recently, the Washington Department of Fish and Wildlife (WDFW) also found high concentrations of PAHs in Puget Sound mussels, especially near areas of moderate to high urbanization (Lanksbury et al. 2014, 2017). Since 2012, WDFW has conducted Puget Sound nearshore contaminant monitoring surveys using transplanted (i.e., caged) mussels, to help track the status and trends of pollution in the marine environment. Washington State will continue to use mussels and other species to monitor toxic contaminants in the Puget Sound to inform pollution control and management efforts in the greater Salish Sea.

References

- Alexander, M.A., Deser, C., and Timlin, M.S. 1999. The reemergence of SST anomalies in the North Pacific Ocean. *J. Clim.* 12: 2419-2433.
- Auth, T.A., Daly, E.A., Brodeur, R.D., and Fisher, J.A. 2018. Phenological and distributional shifts in ichthyoplankton associated with recent warming in the northeastern Pacific Ocean. *Glob. Change Biol.* 24: 259-272.
- Bakun, A. 1990. Global climate change and intensification of coastal ocean upwelling. *Science* 247: 198-201.
- Beaugrand, G., Ibanez, F., and Lindley, J.A. 2003. An overview of statistical methods applied to CPR data. *Prog. Oceanogr.* 58: 235-262.
- Bjorkstedt, E., Goericke, R., McClatchie, S., Weber, E., Watson, W., Lo, N., Peterson, B., Emmett, B., Brodeur, R., Peterson, J., Litz, M., Gomez-Valdez, J., Gaxiola-Castro, G., Lavaniegos, B., Chavez, F., Collins, C.A., Field, J., Sakuma, K., Warzybok, P., Bradley, R., Jahncke, J., Bograd, S., Schwing, F., Campbell, G.S., Hildebrand, J., Sydeman, W.J., Thompson, S.A., Largier, J., Halle, C., Kim, S.Y., and Abell, J. 2011. State of the California Current 2010-2011: Regional variable responses to a strong (but fleeting?) La Niña. *Calif. Coop. Oceanic Fish. Invest. Rep.* 52: 36-68.
- Bograd, S.J., Schroeder, I., Sarkar, N., Qiu, X., Sydeman, W.J., and Schwing, F.B. 2009. Phenology of coastal upwelling in the California Current. *Geophys. Res. Lett.* 36: L01602.
- Bond, N.A., Cronin, M.F., Freeland, H., and Mantua, N. 2015. Causes and impacts of the 2014 warm anomaly in the NE Pacific. *Geophys. Res. Lett.* 42: 3414-3420.
- Brodeur, R.D., Fisher, J.P., Emmett, R.L., Morgan, C.A., and Casillas, E. 2005. Species composition and community structure of pelagic nekton off Oregon and Washington under variable oceanographic conditions. *Mar. Ecol. Prog. Ser.* 298: 41-57.
- Burrows, M.T., Schoeman, D.S., Buckley, L.B., Moore, P., Poloczanska, E.S., Brander, K.M., Brown, C., Bruno, J.F., Duarte, C.M., Halpern, B.S., Holding, J., Kappel, C.V., Kiessling, W., O'Connor, M.I., Pandolfi, J.M., Parmesan, C., Schwing, F.B., Sydeman, W.J., and Richardson, A.J. 2011. The pace of shifting climate in marine and terrestrial ecosystems. *Science* 334: 652-655.
- Checkley, D.M., Asch, R.G., and Rykaczewski, R.R. 2017. Climate, anchovy, and sardine. *Ann. Rev. Mar. Sci.* 9: 8.1-8.25.
- Chhak, K., and Di Lorenzo, E. 2007. Decadal variations in the California Current upwelling cells. *Geophys. Res. Lett.* 34: L14604.
- Crawford, W.R., and Peña, M.A. 2013. Declining oxygen on the British Columbia continental shelf. *Atmos. Ocean* 51: 88-103.
- Daly, E.A., Brodeur, R.D., and Auth, T.D. 2017. Anomalous ocean conditions in 2015: impacts on spring Chinook salmon and their prey field. *Mar. Ecol. Prog. Ser.* 566: 169-182.
- Di Lorenzo, E., and Mantua, N. 2016. Multi-year persistence of the 2014/15 North Pacific marine heatwave. *Nat. Clim. Change* 6: 1042-1048.

- Di Lorenzo, E., Schneider, N., Cobb, K.M., Franks, P.J.S., Chhak, K., Miller, A.J., McWilliams, J.C., Bograd, S.J., Arango, H., Curchitser, E., Powell, T.M., and Riviere, P. 2008. North Pacific Gyre Oscillation links ocean climate and ecosystem change. *Geophys. Res. Lett.* 35: L08607.
- Di Lorenzo, E., Fiechter, J., Schneider, N., Bracco, A., Miller, A.J., Franks, P.J.S., Bograd, S.J., Moore, A.M., Thomas, A.C., Crawford, W., Pena, A., and Hermann, A.J. 2009. Nutrient and salinity decadal variations in the central and eastern North Pacific. *Geophys. Res. Lett.* 36: L14601.
- Foreman, M.G.G., Pal, B., and Merryfield, W.J. 2011. Trends in upwelling and downwelling winds along the British Columbia shelf. *J. Geophys. Res.* 116: C10023.
- Frischknecht, M., Münnich, M., and Gruber, N. 2017. Local atmospheric forcing driving an unexpected California Current System response during the 2015–2016 El Niño. *Geophys. Res. Lett.* 44: 304-311.
- Garcia-Reyes, M., and Largier, J. 2010. Observations of increased wind-driven coastal upwelling off central California. *J. Geophys. Res.* 115: C04011.
- Gladics, A.J., Suryan, R.M., Brodeur, R.D., Segui, L.M., and Filliger, L.Z. 2014. Constancy and change in marine predator diets across a shift in oceanographic conditions in the Northern California Current. *Mar. Biol.* 161: 837-851.
- Gladics, A.J., Suryan, R.M., Parrish, J.K., Horton, C.A., Daly, E.A., and Peterson, W.T. 2015. Environmental drivers and reproductive consequences of variation in the diet of a marine predator. *J. Mar. Sys.* 146: 72-81.
- GLOBEC, U. S. 1992. Eastern Boundary Current Program. Report on Climate Change and the California Current Ecosystem. Report No. 7, Global Ocean Ecosystems Dynamics.
- Horton, C.A. 2014. Top-down influences of bald eagles on common murre populations in Oregon. MS Thesis, Oregon State University.
- Huyer, A. 1983. Coastal upwelling in the California Current System. *Prog. Oceanogr.* 12: 259-284.
- Hyrenbach, D.K., and Veit, R.R. 2003. Ocean warming and seabird communities of the Southern California Current System (1987-98): response at multiple temporal scales. *Deep-Sea Res. Pt. II* 50: 2537-2565.
- Jacox, M.G., Fiechter, J., Moore, A.M., and Edwards, C.A. 2015. ENSO and the California Current coastal upwelling response. *J. Geophys. Res.* 120: 1691–1702.
- Jacox, M.G., Hazen, E.L., Zaba, K.D., Rudnick, D.L., Edwards, C.A., Moore, A.M., and Bograd S.J. 2016. Impacts of the 2015-2016 El Niño on the California Current System: Early assessment and comparison to past events. *Geophys. Res. Lett.* 43: 7072-7080.
- Jacox, M.G., Alexander, M.A., Mantua, N.J., Scott, J.D., Hervieux, G., Webb, R.S., and Werner F.E. 2018. Forcing of multiyear extreme ocean temperatures that impact California Current living marine resources in 2016. *Bull. Amer. Meteorol. Soc.* 99: S27-S33.

- Jones, T., Parrish, J.K., Peterson, W.T., Bjorkstedt, E.P., Bond, N.A., Ballance, L.T., Bowes, V., Hipfner, J.M., Burgess, H.K., Dolliver, J.E., Lindquist, K., Lindsey, J., Nevins, H.M., Robertson, R.R., Roletto, J., Wilson, L., Joyce, T., and Harvey, J. 2018. Massive mortality of a planktivorous seabird in response to a marine heatwave. *Geophys. Res. Lett.* 45: 3193-3202.
- Kahru, M., Kudela, R.M., Manzano-Sarabia, M., and Mitchell, B.G. 2012. Trends in the surface chlorophyll of the California Current: Merging data from multiple ocean color satellites. *Deep-Sea Res. Pt. II* 77-80: 89-98.
- Kahru, M., Jacox, M.G., Lee, Z., Kudela, R.M., Manzano-Sarabia, M., and Mitchell, B.G. 2015. Optimized multi-satellite merger of primary production estimates in the California Current using inherent optical properties. *J. Mar. Sys.* 147: 94-102.
- Kahru, M., Jacox, M.G., and Ohman, M.D. 2018. CCE1: Decrease in the frequency of oceanic fronts and surface chlorophyll concentration in the California Current System during the 2014-2016 northeast Pacific warm anomalies. *Deep-Sea Res. Pt. I* 140: 4-13.
- Kimbrough, K.L., Lauenstein, G.G., Christensen, J.D., and Apeti, D.A. 2008. An assessment of two decades of contaminant monitoring in the Nation's Coastal Zone. Silver Spring, MD. NOAA Technical Memorandum NOS NCCOS 74. 105 pp.
- Lanksbury, J.A., Niewolny, L.A., Carey, A.J., and West, J.E. 2014. Toxic contaminants in Puget Sound's nearshore biota: A large-scale synoptic survey using transplanted mussels (*Mytilus trossulus*). Final Report from Puget Sound Ecosystem Monitoring Program (PSEMP). WDFW Report Number FPT 14-08.
<https://wdfw.wa.gov/publications/01643/wdfw01643.pdf>.
- Lanksbury, J.A., Lubliner, B., Langness, M., and West, J.E. 2017. Stormwater action monitoring 2015/16 mussel monitoring survey. Final Report from Toxics-focused Biological Observation System (T-BIOS) and Puget Sound Ecosystem Monitoring Program (PSEMP). WDFW Report Number FPT 17-06. <https://wdfw.wa.gov/publications/01925/wdfw01925.pdf>.
- Lavaniegos, B.E., Jiménez-Herrera, M., and Ambriz-Arreola, I. 2019. Unusually low euphausiid biomass during the warm years of 2014-2016 in the transition zone of the California Current. (in revision).
- Mackas, D.L., Batten, S., and Trudel, M. 2007. Effects on zooplankton of a warmer ocean: Recent evidence from the Northeast Pacific. *Prog. Oceanogr.* 75: 223-252.
- Mantua, N.J., Hare, S.R., Zhang, Y., Wallace, J.M., and Francis, R.C. 1997. A Pacific interdecadal climate oscillation with impacts on salmon production. *Bull. Amer. Meteorol. Soc.* 78: 1069-1079.
- McClatchie, S. 2014. Regional fisheries oceanography of the California Current System and the CalCOFI program. Springer Netherlands. 235 pp.
- McClatchie, S., Field, J., Thompson, A.R., Gerrodette, T., Lowry, M., Fiedler, P.C., Watson, W., Nieto, K.M., and Vetter, R.D. 2016. Food limitation of sea lion pups and the decline of forage off central and southern California. *R. Soc. Open Sci.* 3: 150628.
- Mearns, A.J. 2001. Long-term contaminant trends and patterns in Puget Sound, the Straits of Juan de Fuca and the Pacific Coast. Proceedings of Puget Sound Research 2001 – the Fifth Puget Sound Research Conference. Puget Sound Water Quality Action Team, Bellevue, WA.

Morgan, C.A., Zamon, J.E., and Bucher, C.A. 2018. Cruise Report: NWFSC/NOAA Fisheries FV Frosti, Cruise 17-02, 19-28 June, 2018. 48 pp. Available at: <https://www.cbfish.org/Document.mvc/Viewer/P163147>.

Neveu, E., Moore, A.M., Edwards, C.A., Fiechter, J., Drake, P., Crawford, W.J., Jacox, M.G., and Nuss, E. 2016. An historical analysis of the California Current circulation using ROMS 4D-Var: System configuration and diagnostics. *Ocean Mod.* 99: 133-151.

Pena, M.A., and Bograd, S.J. 2007. Time series of the northeast Pacific. *Prog. Oceanogr.* 75: 115-119.

Peterson, W.T., Morgan, C.A., Fisher, J.P., and Casillas, E. 2010. Ocean distribution and habitat associations of yearling Coho (*Oncorhynchus kisutch*) and Chinook (*O. tshawytscha*) salmon in the northern California Current. *Fish. Oceanogr.* 19: 508-525.

Peterson, W.T., Fisher, J.L., Strub, P.T., Du, X., Risien, C., Peterson, J., and Shaw, C.T. 2017. The pelagic ecosystem in the Northern California Current off Oregon during the 2014-2016 warm anomalies within the context of the past 20 years. *J. Geophys. Res.* 122: 7267-7290.

Robertson, R., and E.P. Bjorkstedt. 2020. Climate-driven variability in *Euphausia pacifica* size distributions off northern California. *Progress in Oceanography* 188:102412

Rudnick, D.L., Zaba, K.D., Todd, R.E., and Davis, R.E. 2017. A climatology of the California Current System from a network of underwater gliders. *Prog. Oceanogr.* 154: 64-106.

Rykaczewski, R.R., and Checkley, Jr., D.M. 2008. Influence of ocean winds on the pelagic ecosystem in upwelling regions. *Proc. Nat. Acad. Sci. USA* 105: 1965-1970.

Rykaczewski, R.R., Dunne, J.P., Sydeman, W.J., Garcia-Reyes, M., Black, B.A., and Bograd, S.J. 2015. Poleward displacement of coastal upwelling-favorable winds in the ocean's eastern boundary currents through the 21st century. *Geophys. Res. Lett.* 42: 6424-6431.

Sakuma, K.M., Field, J.C., Mantua, N.J., Ralston, S., Marinovic, B.B., and Carrion, C.N. 2016. Anomalous epipelagic micronekton assemblage patterns in the neritic waters of the California Current in spring 2015 during a period of extreme ocean conditions. *Calif. Coop. Oceanic Fish. Invest. Rep.* 57: 163-183.

Sydeman, W.J., Garcia-Reyes, M., Schoeman, D., Rykaczewski, R.R., Thompson, S.A., Black, B.A., and Bograd, S.J. 2014. Climate change and wind intensification in coastal upwelling ecosystems. *Science* 345: 77-80.

Thayer, J.A., MacCall, A.D., Davison, P.C., and Sydeman, W.J. 2017. California anchovy population remains low, 2012-2016. *Calif. Coop. Oceanic Fish. Invest. Rep.* 58: 69-76.

Thompson A.R., et al. 2018. State of the California Current 2017–18: Still not quite normal in the North and getting interesting in the South. *Calif. Coop. Oceanic Fish. Invest. Rep.* 59: 1-66.

Velarde, E., Ezcurra, E., Horn, M.H., and Patton, R.T. 2015. Warm oceanographic anomalies and fishing pressure drive seabird nesting north. *Sci. Adv.* 1: e1400210.

Zaba, K.D., and Rudnick, D.L. 2016. The 2014–2015 warming anomaly in the Southern California Current System observed by underwater gliders. *Geophys. Res. Lett.* 43: 1241-1248.